NATIONAL AERONAUTICS AND SPACE ADMINISTRATION

Technical Memorandum 33-704

A Free-Flight Investigation of Transonic Sting Interference

Peter Jaffe

(NASA-CR-142084) A FREE FLIGHT INVESTIGATION OF TRANSONIC STING INTERFERENCE (Jet Propulsion Lab.) $3.75
48 p HC
CSCL 01C
N75-16544
Unclas
G3/05 09626

JET PROPULSION LABORATORY
CALIFORNIA INSTITUTE OF TECHNOLOGY
PASADENA, CALIFORNIA

January 1, 1975

NATIONAL AERONAUTICS AND SPACE ADMINISTRATION

Technical Memorandum 33-704

A Free-Flight Investigation of Transonic Sting Interference

Peter Jaffe

JET PROPULSION LABORATORY
CALIFORNIA INSTITUTE OF TECHNOLOGY
PASADENA, CALIFORNIA
January 1, 1975

Prepared Under Contract No. NAS 7-100
National Aeronautics and Space Administration

PREFACE

The work described in this report was performed by the Applied Mechanics Division of the Jet Propulsion Laboratory.

Preceding page blank

CONTENTS

TABLES

FIGURES

Preceding page blank

ABSTRACT

A unique experimental program designed to investigate transonic sting interference has been conducted in the Ames Research Center's 1.83 x 1.83-m (6 x 6-ft) Supersonic Wind Tunnel. The basis of the program was to obtain free-flight and sting-support data on identical models in the same wind tunnel Five configurations were used in the investigation. The two principal ones, representing fuselage bodies, were cigar-shaped with tail fins. The others were a sharp 10-deg cone, a sphere, and a blunt entry body. The comparative data indicated that the sting had an appreciable effect on the drag for the fuselage-like configurations. The drag rise occurred 0.02 Mach number earlier in free flight, and the drag level was 15% greater. The spheres and the blunt bodies, on the other hand, were insensitive to the presence of stings regardless of their size. The 10-deg cones were in between, experiencing no drag difference with a minimum diameter sting, but a moderate difference with the largest diameter sting tested. Two additional types of unusual information were obtained: base pressure telemetry data from the free-flight models, and high-speed schlieren movies of the flow over the body on the sting. All the data tend to confirm the notion that for the more slender bodies the sting not only affects flow but the forebody flow as well.

I. INTRODUCTION

The current interest in high-performance aircraft capable of cruising very close to Mach 1 has reestablished our concern about the problem of testing in this regime. As regards the support interference aspect of the problem, experimental research has been performed since the midfifties However, other than indicating that there are effects due to supports, the results are inconclusive. The basic problem with the earlier work is that the results could not be quantified because of the inability to completely eliminate supports in the experiments and thus provide an irreproachable frame of reference. In general, the results also were clouded by too many parameters and the inability to separate the effects.

The question of how to avoid these pitfalls suggested a technique that we have used successfully before, the wind tunnel free-flight technique. The basis of it is that models are pneumatically launched in free flight against the oncoming flow of the wind tunnel, providing support-free data. By obtaining data on identical models and test conditions in free flight and on supports, an absolute comparison can be made. This report presents the results of a study employing this approach. In it the difference between sting-support and free-flight drag is used to indicate, and provide a measure of, sting interference. The experimental data was obtained in the Ames Research Center's (ARC's) 1.83x1.83-m (6x6-ft) Supersonic Wind Tunnel during two separate test periods in January and May of 1972. In addition to the direct comparison between sting and free-flight drag, the influence of sting diameter was investigated; further, the difference between free-flight and sting support base pressure was investigated by means of base pressure telemetry measurements.

II. CONFIGURATIONS

The principal configuration of this study was the HIRAD-10, a representative fuselage body that had undergone extensive testing at the Langley Research Center (LRC) in connection with the Center's transonic transport development program (Refs. 1 and 2). In addition, two basic configurations with widely different flow characteristics, a 10-deg (half-angle) cone and a sphere, were tested, and a blunt 60-deg (half-angle) cone, for which there existed a great deal of free-flight data (Ref. 3), was tested.

The first phase in the study was to insure that these configurations could be successfully tested at transonic speeds, i.e., that they could be launched and would fly at angles of attack very close to zero. No difficulty was anticipated for the blunt configurations and the 10-deg cone, but the HIRAD-10 was another matter. Initially, it was desired to perform the main portion of HIRAD-10 testing without fins. However, preliminary tests performed in the JPL 50.8-cm (20-in.) Supersonic Wind Tunnel (SWT) at high subsonic Mach numbers indicated that even if a gold ballast was used, pushing the center of gravity to a point 0.18 diameters from the nose, the finless body was unstable. It was then decided to use a finned version of the HIRAD-10, which had also been tested by LRC; this configuration is denoted H10-F (Ref. 2). To investigate configuration modifications required to accommodate a sting, a modified version of the HIRAD-10, with an enlarged afterbody, was also tested; this is denoted MH10-F. Figure 1 shows the test configurations. All the models were 3.81 cm (1.5 in.) in diameter.

A slight modification of the fins was required because of the large number of fins necessary for the free-flight portion of the test. The Langley fins had biconvex airfoil sections whose thickness to chord ratio was 0.03. The fins used in this program had wedge-shaped leading and trailing edges. They were made by machining 7°40' wedge edges on a 0.1588-cm- (0.0625-in.-) thick fin blank of lamicoid. The thickness-to-chord ratio was 0.03 at the maximum chord, but larger on the remainder of the fin.

All of the configurations except the 60-deg blunt cone employed boundary layer trips. Glass beads were used for the tripping mechanism. The bead diameters, trip widths and positions were determined by a formula given in Ref. 4. In the case of the HIRAD configurations the trip consisted of 0.0076-cm (0.003-in.) (nominal) beads loosely spaced on a 0.254-cm- (0.1-in.-) wide strip placed 1.27 cm (0.5) in.) from the nose. The 10-deg cone trip used 0.013-cm (0.005-in.) beads on a 0.254-cm (0.1-in.) strip, 1.27 cm (0.5-in.) from the nose. The sphere had 0.0076-cm (0.003-in.) beads loosely spaced over the entire body; the reason for this was that in free-flight the center-of-gravity positions were at the geometric centroid and consequently the orientation of the spheres could not be predetermined.

III. STING-SUPPORT TEST

All of the sting-support data were obtained on a 1.27-cm- (0.5-in.-) diameter TASK six-component strain gage balance having a maximum permissible chord force of 22.2 N (5 lb). The HIRAD models were constructed so that the balance was in a cavity forward in the body and mated with a sting that necked down to 0.792 cm (0.312 in.) at the base. From the model base the sting grew to a 1.27-cm (0.5-in.) diameter in 26.7 cm (10.5 in.) and connected with the tunnel sting. A typical HIRAD installation is shown in Fig. 2. The other models used the same sting but were mounted further forward. The distance to the model base was an additional 12.4 cm (4.9 in.) for the 10-deg cone, 14.7 cm (5.8 in.) for the sphere, and 17.5 cm (6.9 in.) for the 60-deg blunt cone. For these three configurations a large portion of the balance protruded out of the base and had to be covered with a wind-shield. Different diameter stings were simulated with different diameter wind-shields. Table 1 contains this information.

The balance was calibrated in a standard manner by the Ames Research Center's calibration instrumentation group. The nominal accuracy of the balance was 0.5% of full scale or 0.11 N (0.025 lb) in drag. This turns out to be between 0.5 to 1.5% of the coefficient value for most of the test conditions. In general, the overall data accuracy was more governed by the unsteadiness of the flow than by the balance accuracy; this will be discussed later.

During the first sting support test, data was obtained on the two HIRAD configurations, the 10-deg cone, the sphere, and the 60-deg blunt cone. The test parameters were sting diameter, Mach number, and Reynolds number.

Typically, the data were obtained in the angle-of-attack range of ±1.0 deg. For each configuration, one run, at a middle Mach number, was made for angles of attack up through 8.0 deg. A summary of the test conditions are shown in Table 1.

Figure 3 shows the near zero angle-of-attack sting support drag data (nominally -1.0 to +1.0 deg) for Configuration H10-F obtained during the first test. Also included on the plot are the corresponding base pressure coefficients, C_{p_b}'s. C_{D_T} is the total drag coefficient as measured by the balance; no base pressure correction has been made. Each square represents a composite minimum drag value for a run obtained by applying engineering judgment to the angle-of-attack/drag data. The points surrounding the square are the data that went into forming those values with no regard for the angle-of-attack, but only the Mach number. Each point is the result of averaging five scans of balance and tunnel condition readings over a period of about 1.2 s. This process was used to insure that the natural cyclic variation in the tunnel, which was about 0.85 Hz, was accounted for. From the data it appears that the Mach effect is much stronger than the angle-of-attack effect and, therefore, the best way to describe the situation is to use the Mach value and ignore the angle-of-attack. In the second test this knowledge was taken advantage of, and testing was performed only at zero angle of attack.

Included on the plot are data points taken slightly below and above the principal Reynolds numbers, 0.91×10^6/m (3.0×10^6/ft), and the base pressure data for all of the runs. The slight variation in Reynolds number seemed to have little or no influence on the data. The base pressure on the HIRAD models was obtained by measuring the pressure in the balance cavity by means of a hole within the sting that exited at the balance/sting junction. For the other configurations a small line on the side of the sting provided the base pressure data.

The data on the other four configurations are shown in Figs. 4 through 7. Except for the 60-deg blunt cone, data was obtained with two different sting diameters; both sets are shown on the same plot.

Visual schlieren observations obtained during the test indicated that the flow was very unsteady and constantly changing, particularly in the Mach region of 0.98 to 1.05. The model and sting were also oscillating sometimes rather violently with an amplitude of as much as a few centimeters. To investigate this unsteadiness, 35-mm high-speed movies were taken of the flow through the schlieren system with the same photo setup as was used during the free-flight portion of the test. From the movies it appeared that the flow in the wake/afterbody region was in a constant state of flux, oscillating between a band of Mach numbers. Over the long term, the higher Mach number flow was dominant. This was determined from the wake shock angle. By studying the films and comparing them with free-flight films it was possible to determine the variation in Mach number for a typical oscillation. Figure 8 shows a comparison of the flow over a 10-deg cone.

In this example the sting support Mach number varied 0.03 but favored a Mach number close to nominal. Typically the Mach variation was smaller, somewhat greater than 0.01. This also corresponds fairly well to the delta Mach number indicated by the data scanning process. In addition to the Mach variation, there appeared to be a great deal of spurious flow, the origin of which was too difficult to determine. Comparisons with the free-flight movies indicated that there was a substantially greater amount of this activity with the sting-support models.

Some five months after the first test the balance was recalibrated and installed in the tunnel, the boundary layer transition grit was reapplied, and another force test performed. The purpose of the second test was to fill in and expand upon the results from the first test and to obtain a confirmation of those results. During the second test, greater emphasis was placed on determining the proper Mach number and drag by taking more samples per data point. Figures 9 and 10 contain the second test data points for configurations H10-F and the 10-deg cone. The curves on the plots are the mean results from the first test. As can be seen, the comparison of the H10-F results is excellent. The 10-deg cone comparison is good before the drag rise and then becomes poorer. The difference, in part, may be due to slightly different minimum sting diameters. During the first test the sting diameter was 1.42 cm (0.56 in.) and during the second, 1.60 cm (0.63 in.). The difference between the two sets of 2.54-cm (1-in.) sting data is a little baffling, particularly in view of the excellent H10-F comparison. Unfortunately, this did not come to light until after the test. Configurations MH10-F, the sphere, and the 60-deg blunt cone were not retested.

Some general observations: The HIRAD data, per design, shows a negligible Mach effect prior to Mach 0.96. After that the curve abruptly peaks and unexpectedly dips down and rises again. The reverse occurs with the base pressures, which look somewhat like mirror reflections of drag curves. The base pressure coefficients with the 0.792-cm (0.312-in.) sting were positive on both configurations. However, with the 1.91-cm (0.75-in.) sting the MH10-F data was more negative. Both the sphere and cone data appear to be well behaved. In the case of the sphere, there is a long drag creep from the subsonic level and then a sharp rise beginning at Mach 0.96. The incompressible subsonic drag value occurs below the minimum Mach number tested, Mach 0.8. The base pressure coefficients for both these configurations were strongly negative.

In all cases where more than one sting diameter was used, with the exception of the sphere, there was a substantial difference in the total drag. To look at this in more detail a comparison of the forebody drag coefficient, C_{D_F}, for Configuration MH10-F and the 10-deg cone are shown in Figs. 11 and 13. Figure 12 also contains a forebody drag comparison of Configurations H10-F and MH10-F with the 0.792-cm (0.312-in.) sting. Forebody drags were obtained by subtracting the base drag, as determined from the base pressure data, from the total drag. The MH10-F comparison (Fig. 11) indicates a strong influence of sting diameter throughout the Mach regime tested, particularly at the lower Mach numbers where the drag with the smaller sting was about 13% greater. In addition to the level difference, the drag rise occurred earlier with the smaller sting. The comparison between the H10-F and MH10-F data (Fig. 12) indicates that Configuration H10-F has a drag level 7% greater before the drag rise. The rise also occurred earlier with H10-F, as did the characteristic peak and dip. The overall level after the rise was about the same for both configurations. A comparison of the total drag between these two configurations shows about the same result. Unfortunately, it is not clear what part of the difference was due to altering the afterbody geometry, and what part was due to having a step between the base and sting. However, a comparison of drag between Configuration H10-F with the 0.792-cm (0.312-in.) sting, and Configuration MH10-F with the 1.91-cm (0.75-in.) sting (not shown), where there was no step, indicates a much greater disagreement, thus pointing toward geometry as having the larger influence.

The 10-deg cone comparison (Fig. 13) indicates a rather surprising result. During the drag rise the forebody drag difference was small, but, prior to and after it, the difference was quite large. At Mach 0.8 the forebody drag with the larger sting was 16% greater. Even though there is a step between the base and sting it appears that the large sting influences the forebody pressure distribution and consequently the forebody drag.

A disturbing result from the program was the lack of agreement between the H10-F results and data obtained by the Langley Research Center on an almost identical configuration (Ref. 2) during a rather extensive test program. As indicated earlier, the only difference between the configurations during the two test programs was the fins. Figure 14 shows the comparative data from the two programs. Not shown on the figure was the base pressures, which correlated reasonably well.

In an endeavor to solve this disparity two things were done. First, data was obtained on the H10-F without boundary layer trips to see what influence this had. Second, the influence of the fins was investigated. The results from the no-trip survey indicated a drag level well below both the trip level and the LRC data. The value at Mach 0.9 was 0.077. One possibility for the disparity, therefore, was a difference in the comparative states of the boundary layers and (or) the turbulence levels in the tunnels. In an attempt to determine if the fins could be the reason for the difference, a slightly longer finless configuration, and one that was previously tested in the LRC 2.44-m (8-ft) Transonic Tunnel, was tested. The comparison between the 1.83 x 1.83-m (6 x 6-ft) wind tunnel data and the LRC results on a series of different blockage models is shown in Fig. 15, where A_M/A_T is the ratio of the model-to-tunnel cross-sectional area, and d_s/d_{max} is the ratio of the sting diameter to maximum body diameter. Again the disagreement is quite large and in the same direction as before. This tends to discount the probability that the disparity was due to the fins. One notable difference between the two sets of data, however, was the blockage. As indicated on the figure, blockage during the 1.83 x 1.83-m (6 x 6-ft) wind tunnel tests was much smaller. Also, the LRC data on the plot shows a trend of increasing drag with decreasing blockage even for very small blockage ratios. It is possible that the 1.83 x 1.83-m (6 x 6-ft) wind tunnel data may be consistent with the LRC results and that blockage may be the culprit. Obviously, more work needs to be done in this area.

IV. FREE-FLIGHT TEST

There are three essential ingredients required to perform free-flight tests in the wind tunnel: a launch gun capable of imparting the proper velocity to the model, a viewing area in the test section sufficiently large to provide model motion data, and a movie camera capable of recording the motion. In regards to the gun, a considerable amount of free-flight work has already been done in the 1.83 x 1.83-m (6 x 6-ft) wind tunnel and fortunately a gun was already available (Ref. 3). The 1.83 x 1.83-m (6 x 6-ft) wind tunnel has large circular viewing windows, some 117 cm (46 in.) in diameter, providing excellent coverage of the flights. The optical quality of the windows was poor, but, except for degrading the schlieren effect, its influence on the free-flight data was small. The movie camera employed is one that is used at JPL, a PhotoSonics 35-mm full-frame camera. It was installed in the tunnel so that the photographs could be taken through the schlieren system, thereby eliminating parallax distortions. During the tests the camera was operated at about 2000 frames/s. In the sequencing of events the camera was started first and allowed to accelerate up to speed. After 2 s the gun was fired, and then the gathering of the tunnel information was initiated and the pertinent pressures midway in the flight recorded. During the second test this information was recorded prior to, during, and after the flight so that a better appraisal of the proper Mach number could be made.

The design of the free-flight models was particularly difficult. In addition to providing acceptable mass characteristics for both acceleration and stability, stringent requirements about the structure were placed on the design. The exterior of the models had to be made of relatively soft material compared with the tunnel and the ballast was required to break into small pieces upon impact with the tunnel. This was necessary for safety, to insure that a solid mass would not impact one of the compressor blades. The solution to the ballast problem was the use of powdered lead for the 10-deg cones and spheres, and a series of lead washers for the HIRAD models. The cone exterior shells were extruded plastic, and for the sphere exteriors, ping-pong balls were used. The HIRAD bodies were made of sugar pine on a template follower lathe; a cavity along the centerline at the nose was provided to hold the ballast. Once the ballast was inserted a wood plug sealed the cavity and the nose was finished. Figure 16 contains a schematic showing the construction of the models, and Fig. 17 shows an H10-F model mounted on the launch gun ready for launching. Table 2 contains typical model mass characteristics and pertinent flight conditions. For simplicity the flight information is given for one Mach number, 1.02.

Free-flight data was obtained during both test periods. All together some 60 shots were made; of these, 52 were reduceable. Figure 18a shows a short flight sequence with Configuration MH10-F. Only every 20th frame of data is shown. This run, which was typical, had over 300 frames of data. The time interval between photos is approximately 0.01 s. Figures 18b, 18c, and 18d contain typical frames of data with the other configurations. From the film data the translational positions were read and related to a time base that was independently placed on the edge of the film by a 0.001-s pulse generator. This data was processed by computer to a velocity/distance history, and from there to drag as indicated below.

The instantaneous drag coefficient is defined as (Ref. 5).

$$C_D = \frac{-2m}{\rho A} \frac{d\left[\ln\left(1 - V_m/V_\infty\right)\right]}{dx} \tag{1}$$

Where V_m is the model velocity, V_∞ is the free-stream velocity, x is the relative distance between the model and flow, m is the model mass, ρ is the flow density, and A is the model reference area. It is obvious from Eq. (1) that if the drag coefficient is constant a plot of $\ln(1 - V_m/V_\infty)$ versus x will be linear. Changes in the drag coefficient during the flight are reflected in changes in the slope. Figure 19 contains a ln plot for the run of the sequence shown in Fig. 14a. For clarity only every second point is shown. As indicated, the data appears to be linear. Included on the plot are the mean straight line fits. The maximum possible deviation of the slope is 1.5%. In terms of the drag coefficient this amounts to about 0.002. A 1.0% error value is fairly representative of all the HIRAD flights. For the cones and spheres the accelerations were considerably greater and as a result the scatter was much smaller. Initially it was thought that by curve fitting the cone and sphere $\ln(1 - V_m/V_\infty)$ data the instantaneous drag history for each flight could be determined. In practice it turned out that the film data was not sufficiently accurate to do this. Instead, it appeared best to obtain one mean drag value per flight. As a result all of the cone and sphere data (as well as the HIRAD data) are presented as effective constant drag coefficients.

One of the critical requirements was that the models fly very close to a zero angle-of-attack to permit an unqualified comparison with the sting supported data. In general this requirement was met. For the 10-deg cones (and, of course, for the spheres that had no orientation) there was no difficulty, but the HIRAD Configurations' angle-of-attack oscillatory motion occasionally exceeded 5 deg; those runs were discarded. Of the remaining runs most of them fell below 3 deg, and many of these were less than 2 deg. Between 3 deg and 5 deg an adjustment was made with the H10-F sting-support drag data shown in Fig. 20. Below 3 deg no correction was made since for a vehicle oscillating ±3 deg the effective angle-of-attack, in terms of drag, is $1/\sqrt{2}$ times 3 deg or 2.12 deg. This amounts to an error in the drag coefficient (from Fig. 20) of approximately 0.004 in the positive direction. Adding this to the error in determining the ln $(1-V_m/V_\infty)$ slope amounts to an overall error of -1.5 to +4.0% for the zero angle-of-attack HIRAD free-flight drag coefficients. This is a maximum possible value; a more realistic value for the data as a whole is ±1.5%.

Figures 21 through 25 contain a summary of all the free-flight data reduced as well as the corresponding minimum diameter sting-support data. The support data is the composite from both tests. The numbers next to the points are the run numbers; numbers greater than 35 were runs obtained during the first test. The 60-deg blunt body free-flight data was obtained during an earlier program (Ref. 3). Included on the blunt body plot are data from a variety of sources, an atmospheric flight, several ballastic ranges, and another wind tunnel. Except for the ARC 0.61 x 0.61-m (2 x 2-ft) Transonic Tunnel data (Ref. 6), the overall agreement from the different facilities is reasonably good.

For purposes of discussion, the comparative results are broken up into three categories: high-drag configurations, which contain the spheres and 60-deg blunt bodies; low-drag simple geometry configurations, which contain the 10-deg cones; and low-drag complex geometry configurations, which contain the HIRAD bodies.

A. HIGH-DRAG CONFIGURATIONS

Figures 21 and 22 contain the comparison between free-flight and sting-support drag for the two blunt bodies. The comparison of the data for both configurations is quite good, particularly the sphere data where all but one free-flight point falls within the combined experimental scatter of the two techniques. This result is not surprising since, from the sting-support data (Fig. 6), the data obtained with two widely different sting diameters shows good agreement. From the schlieren photographs it appears that a shock is established at or near the maximum diameter point regardless of whether a sting was present or not. This tended to do two things: retain and fix the forebody pressure profile, and blanket the whole base area. Couple this with an inherently low base pressure and a large forebody pressure and a situation is generated where total drag force is insensitive to base protrusions. It appears that if reasonable-size stings are used, there will be very little measurable altering of the flow and consequently of the drag for these configurations.

B. LOW-DRAG SIMPLE GEOMETRY CONFIGURATIONS

The excellent agreement between the free-flight and minimum diameter sting drag data for the 10-deg cone (Fig. 23) indicates that when a sufficiently small (but reasonable size) sting is used the interference effects can be made unimportant. However, had the free-flight data been compared with the 2.54-cm- (1-in.-) diameter sting data, the conclusion would have been different. As indicated by the sting support data, the flow field is sensitive to the size of the sting. The question that must be asked is whether the larger sting influences only the base region or whether it affects the forebody region as well? From the base pressure data (Figure 10) and the forebody drag comparison (Figure 13), the answer is clear. If the stings were affecting the base region, the forebody drags would agree with one another, but they did not. The base drags were obtained from the corresponding sting base pressure data shown in Fig. 10. If instead it was assumed that the 1.42-cm (0.56-in.) sting base pressure data was the correct set for both stings and it was used to obtain the forebody drag for the 2.54-cm- (1.0-in.-) diameter sting, the correlation would be even worse.

The main conclusions are that this class of configurations can be successfully tested with a sting after an exploratory investigation is performed to determine the proper sting-to-base diameter ratio, and that determining the proper base pressure coefficient is not sufficient to correct for the presence of the sting.

C. LOW-DRAG COMPLEX GEOMETRY CONFIGURATIONS

This category presents the most difficulty. The H10-F comparison (Fig. 24) definitely shows a strong difference between the two sets of data. The onset of the free-flight drag rise occurs 0.02 Mach number sooner and the level is 15% greater.* The surprising feature is that the drag level

---

*What does this mean in terms of an aircraft? If it is assumed that the interference manifests itself only on the drag of the fuselage and that the fuselage drag makes up 0.1 of the total drag, this still amounts to a significant ΔC_D of 0.015.

difference persists well below the drag rise region throughout the Mach range tested, i.e., at least down to Mach 0.85. Interestingly, the H10-F free-flight points appear to match up fairly well with the MH10-F/0.792-cm (0.312-in.) sting data. Of course, this might just be a coincidence. The MH10-F free-flight/minimum sting comparison (Fig. 25) also shows about the same level difference but does not indicate the early onset of the drag rise. The level difference is also compatible with the results from the two sets of sting data that have both been included on the Figure. The effects of sting diameter at Mach 0.9 for the three available data points, 0.792-cm- (0.312-in.-) diameter sting, 1.91-cm- (0.75-in.-) diameter sting, and zero-diameter sting (free flight), are shown on Fig. 26. Delta C_D is the difference between the sting drag and the free-flight drag. The trend between free-flight and small sting, and small sting and large sting, is quite well behaved, providing additional credence to the whole analysis.

The flow fields about these configurations are noteably different from the others; the recompression shock, which occurs in the wake on the other configurations, occurs on the afterbody of these. As a consequence, the pressure in the afterbody/base area is considerably greater. Add to this a sting whose size relative to the base is large because of the test requirements and the result is an altering of the flow upstream of the base. It should be noted that having the recompression shock on the body and having to contend with a fairly large sting-to-base diameter ratio is the situation found on most fuselage configurations; consequently, this same effect could be expected with them as well.

During the test, two free-flight runs were made with Configuration H10-F having 7.62-cm- (3-in.-) long simulated sting protrusions. One of the runs had a large angle-of-attack oscillation and had to be discarded. The other, Run 106, is included on Fig. 21. Although it is dangerous to place too much credence in one data point, this point falls very close to the sting support data and suggests that: (1) sting effects can be simulated in free-flight, and (2) the near sting has the dominant influence on the flow. Obviously, more work along these lines should be performed.

V. BASE PRESSURE TELEMETRY

The comparative free-flight/sting-support data indicate that for some configurations the presence of the sting alters the flow resulting in a change in drag. A question that must be addressed is: can the apparent sting interference be rectified by merely determining the proper base pressure and making the appropriate correction, or does the sting alter the pressure profile along the body making such a correction inappropriate. This latter conclusion was alluded to before in the comparison of forebody drag but, to pin it down more firmly, a unique set of experiments were conducted during the second test. During the test, free-flight base pressure data was obtained by means of telemetry; all together about a dozen of the free-flight models were equipped with telemetry devices.

The telemetry units consisted of an FM transmitter based on a Calpitts oscillator circuit coupled with a 3.45-N/cm^2 differential (5-psid) Kulite full-bridge transducer. The reference side of the transducer was capped and the leak rate adjusted, not to exceed 2% of 0.69 N/m^2 (1 psi) full scale in 200 μs, which was about the nominal duration of a flight. Thus, the transducer reference pressure was quasi-steady during each flight. This pressure was measured prior to the launching of the model by means of a loose line connecting the launch pad and tunnel. At launch the line was disengaged by the launch action. Just prior to and during the flight the signal from the telemetry unit was recorded on an oscillograph.

Most of the data was obtained with the two HIRAD Configurations. Figure 27 shows an MH10-F assembled telemetry model; below the model are shown the individual components. The components were packaged in a plastic sleeve that fit into a cavity in the model. The telemetry models weighed slightly more than the regular models, and the center-of-gravity positions were the same (see Table 2). A few of the 10-deg cones were also fitted with telemetry units. However, because of a variety of problems from electronic malfunctions to large oscillations undoubtedly due to a relaxation of the center-of-gravity position to accommodate the telemetry package, only one good data point was obtained, and because there is no statistical confirmation of its validity, it is not presented.

Within an hour of their use, the internal battery packs were hard wired to the transducer/transmitter assemblies and calibrated with a three-point pressure pulse, which was intended to somewhat simulate the pressure changes that were to occur during the flight. Prior to this preflight calibration, during manufacture, all units were tuned to the FM band at 110 to 114 MHz. Sample calibrations on telemeters during manufacture indicated a 2% deviation in sensitivity at 0.69 N/cm^2 differential (1 psid) and 4% hystersis during a negative and positive calibration. In general the preflight calibrations were not as good as this. The range of possible calibration slopes deviated typically 4% and occasionally as high as 7%, causing the same percentage of uncertainty in the base pressure. In terms of the base pressure coefficients this means generally larger variations depending upon the reference and static pressures.

The telemetry data was synchronized to the flight by two methods: the initiation of a 60-cycle signal indicating that the gun had been fired, and a photocell device that indicated that the model passed the entry edge of the viewing window. The second method only worked sporadically but fortunately the first method provided sufficient information. All of the pertinent data were recorded on the same oscillograph trace; a typical trace is shown in Fig. 28. All of the HIRAD telemetry data are presented in Fig. 29 as well as the sting-support data.

Even though there was an excessive amount of scatter in the data, the trend seems clear; for both configurations the telemetry base pressure was at about the same level or more positive than the static base pressure. In terms of correcting the drag this would have the opposite effect. A positive delta pressure on the base would result in a force opposing the drag force and would consequently reduce the sting drag by that amount making the disparity between the sting data and the free-flight data even greater.
To correct the sting data at Mach 0.9, for instance, a telemetry base pressure coefficient value 0.3 smaller would have had to have been obtained.

VI. CONCLUSIONS

The presence of a sting during transonic testing will influence the drag to a greater or lesser degree, depending upon the configuration of the model. In the case of the fuselage-like configurations this effect was severe. The comparative free-flight and sting-support data obtained during the test program showed the drag rise occurring 0.02 Mach number late and the drag level 15% smaller with the sting. A surprising feature was that the drag level difference persisted well below the drag rise region, at least down to Mach 0.85, the lowest Mach number tested. In terms of aircraft performance this could result in 10 to 20 drag counts.

The three other configurations tested, sharp 10-deg cones, spheres, and 60-deg blunt entry bodies, experienced smaller to no effects. In the case of the sharp 10-deg cones, the effect was appreciable with a moderate-size sting ($d_s/d = 0.67$), and became negligible with the minimum diameter sting tested ($d_s/d = 0.37$). Both blunt configurations, on the other hand, were insensitive to the presence of the sting, and, for the most part, the sting diameter.

In general, sting interference appears to be more than just a base phenomenon. All of the diagnostic factors, sting forebody drag, comparisons between free-flight telemetry and sting base pressure, and high-speed and regular flow visualization all point to the forebody flow being influenced by the presence of the sting.

REFERENCES

1. Couch, L.M., "Transonic Wall Interference Effects on Bodies of Revolution," paper No. 72-1008 presented the AIAA 7th Aerodynamic Testing Conference, Palo Alto, California, September 13–15, 1972.

2. Ursy, J. W., and Wallace, J. H., Drag of a Supercritical Body of Revolution in Free Flight at Transonic Speeds and Comparison with Wind-Tunnel Data, Technical Note TN D-6580. National Aeronautics and Space Administration, Washington, D. C., December 1971.

3. Marko, W. J., Transonic Dynamic and Static Stability Characteristics of Three Blunt-Cone Planetary Entry Shapes, Technical Report 32-1357. Jet Propulsion Laboratory, Pasadena, California, September 1, 1969.

4. Tanner, D. D., Simplified Method for Determination of Critical Height of Distributed Roughness Particles for Boundary Layer Transition in the ARO-Operated Facilities at Ames, Technical Memorandum Number 35. ARO, Inc., Moffett Field, California, October 4, 1971.

5. Prislin, R. H., Free-Flight and Free-Oscillation Techniques for Wind-Tunnel Dynamic-Stability Testing, Technical Report 32-878. Jet Propulsion Laboratory, Pasadena, California, March 1, 1966.

6. Marko, W. J., Static Aerodynamic Characteristics of Three Blunted Sixty-Degree Half-Angle Cones at Mach Numbers From 0.60 to 1.30, Technical Report 32-1298. Jet Propulsion Laboratory, Pasadena, California, July 1, 1968.

7. Sammonds, R. I., Dynamics of High-Drag Probe Shapes at Transonic Speeds, Technical Note TN D-6489. National Aeronautics and Space Administration, Washington, D. C., September 1971.

8. Whitlock, C. H., and Benduva, R. J., Dynamic Stability of a 4.6-Meter-Diameter 120° Conical Spacecraft at Mach Numbers from 0.78 to 0.48 in a Simulated Martian Environment, Technical Note D-4558. National Aeronautics and Space Administration, Washington, D.C., May 1968.

9. Krumins, M. V., "Drag and Stability of Mars Probe/Lander Shapes," AIAA J. Spacecraft and Rockets, Vol. 4, No. 8, p. 1052, August, 1967.

Table 1. Sting-support test conditions

Configuration	Sting diameters, cm (inches)	Sting/base ratio	Mach range	Re/m (Re/ft) $(\times 10^6)$
H10-F	0.792 (0.312)	0.80	0.8-1.1	0.762, 0.914, 1.067 (2.5, 3.0, 3.5)
			0.7-1.2[a]	0.914 (3.0)
MH10-F	0.792 (0.312)	0.416	0.8-1.1	0.914 (3.0)
	1.91 (0.75)	1.0	0.8-1.1	0.914 (3.0)
10-deg cone	1.42 (0.56)	0.373	0.8-1.1	0.762 (2.5)
	1.59 (0.625)[a]	0.417	0.7-1.2	0.762 (2.5)
	2.54 (1.00)	0.667	0.8-1.1	0.762 (2.5)
			0.7-1.2[a]	0.762 (2.5)
				0.762 (2.5)
Sphere	1.42 (0.56)	–	0.8-1.5	0.610 (2.0)
	1.91 (0.75)	–		0.610 (2.0)
60-deg blunt cone	1.91 (0.75)	0.5	0.7-1.1	0.457 (1.5)

[a] Second test.

Table 2. Typical mass characteristics and flight conditions at Mach 1.02

Configuration	Mass, (g)	Center-of-gravity, diameters from nose	Re/m (Re/ft) ($\times 10^6$)	Dynamic pressure N/m^2 (lb/ft^2)	Acceleration (a/g)	Flight time, (s)
H10-F	228	3.25	0.914 (3.0)	209 (506)	3.6	0.45[a]
MH10-F	228	3.25	0.914 (3.0)	209 (506)	3.5	0.46[a]
10-deg cone	73	1.30	0.762 (2.5)	173 (419)	18.9	0.20
Sphere	110	0.50	0.610 (2.0)	137 (332)	15.0	0.22

[a] The HIRAD models dropped out of view after about 0.3 s due to gravity.

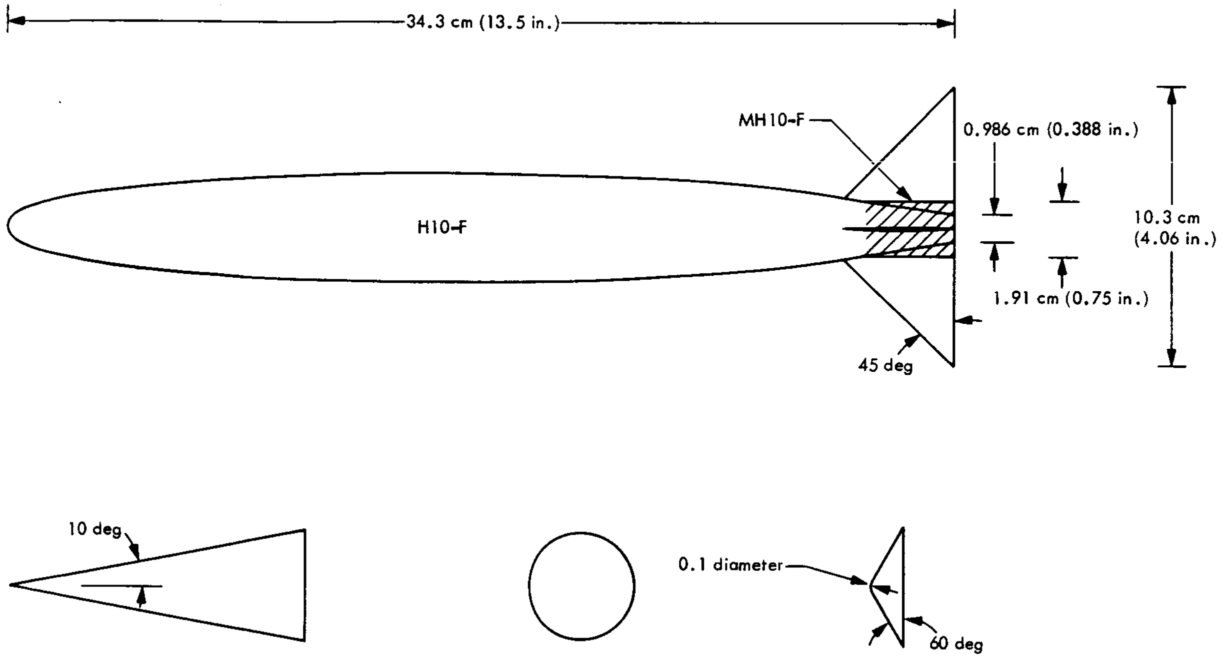

Fig. 1. Test configurations

Fig. 2. Sting-support test installation

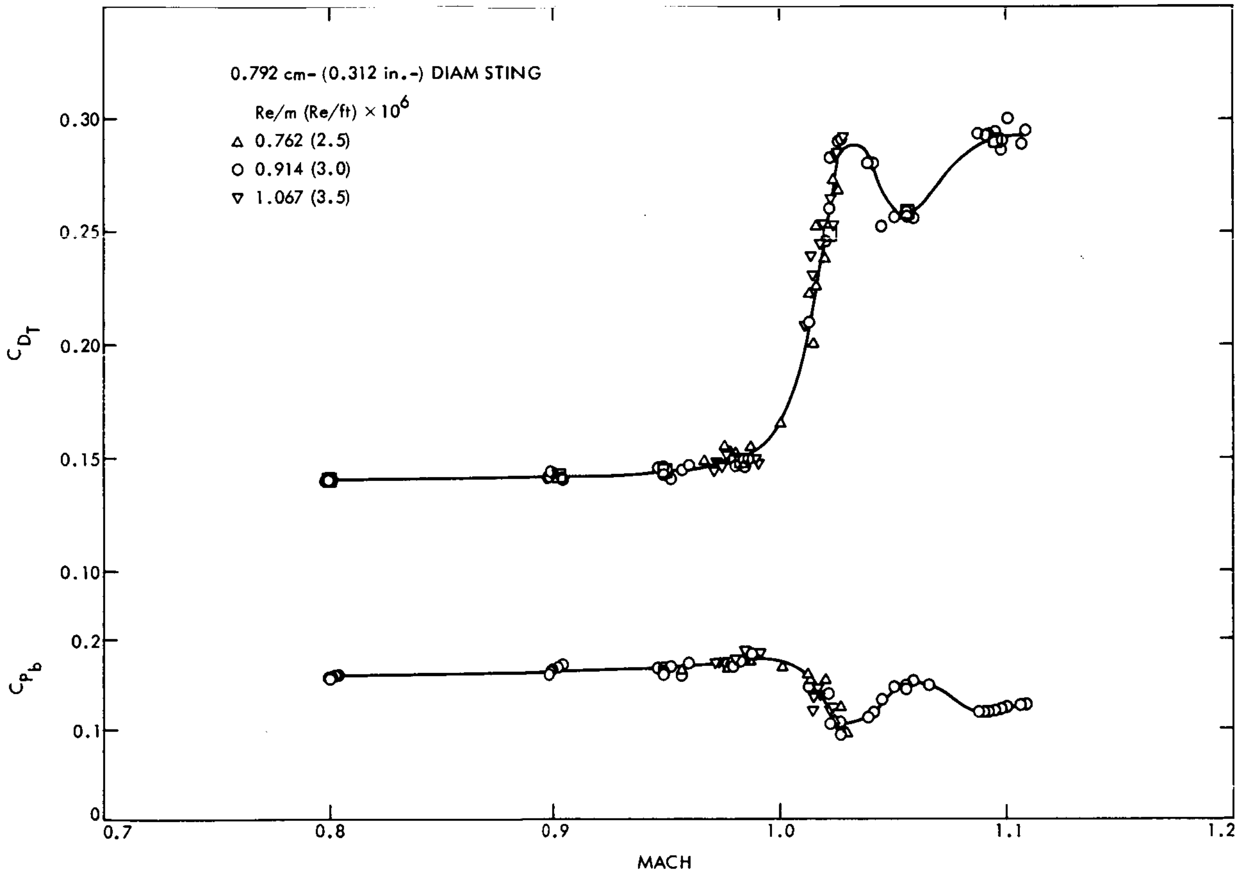

Fig. 3. Configuration H10-F sting-support drag

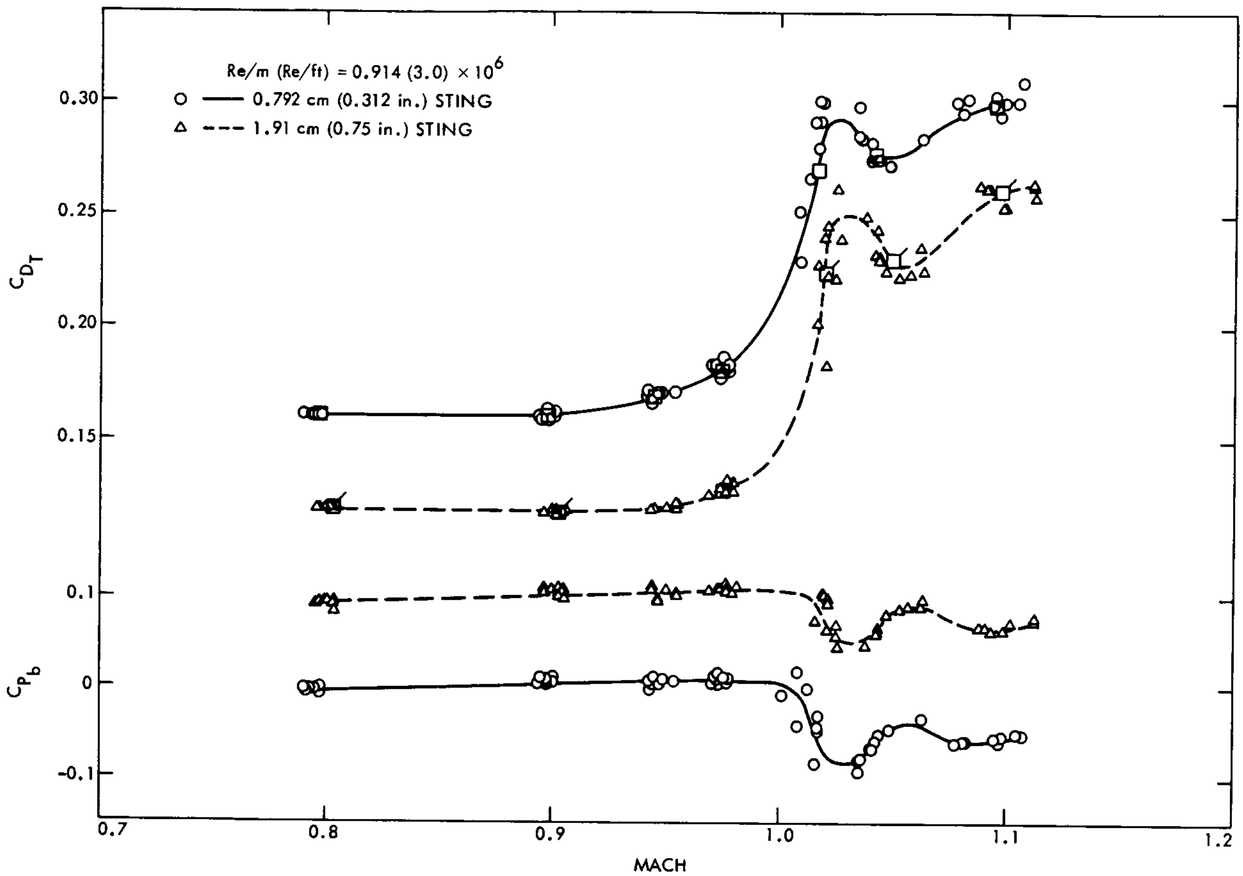

Fig. 4. Configuration MH10-F sting-support drag

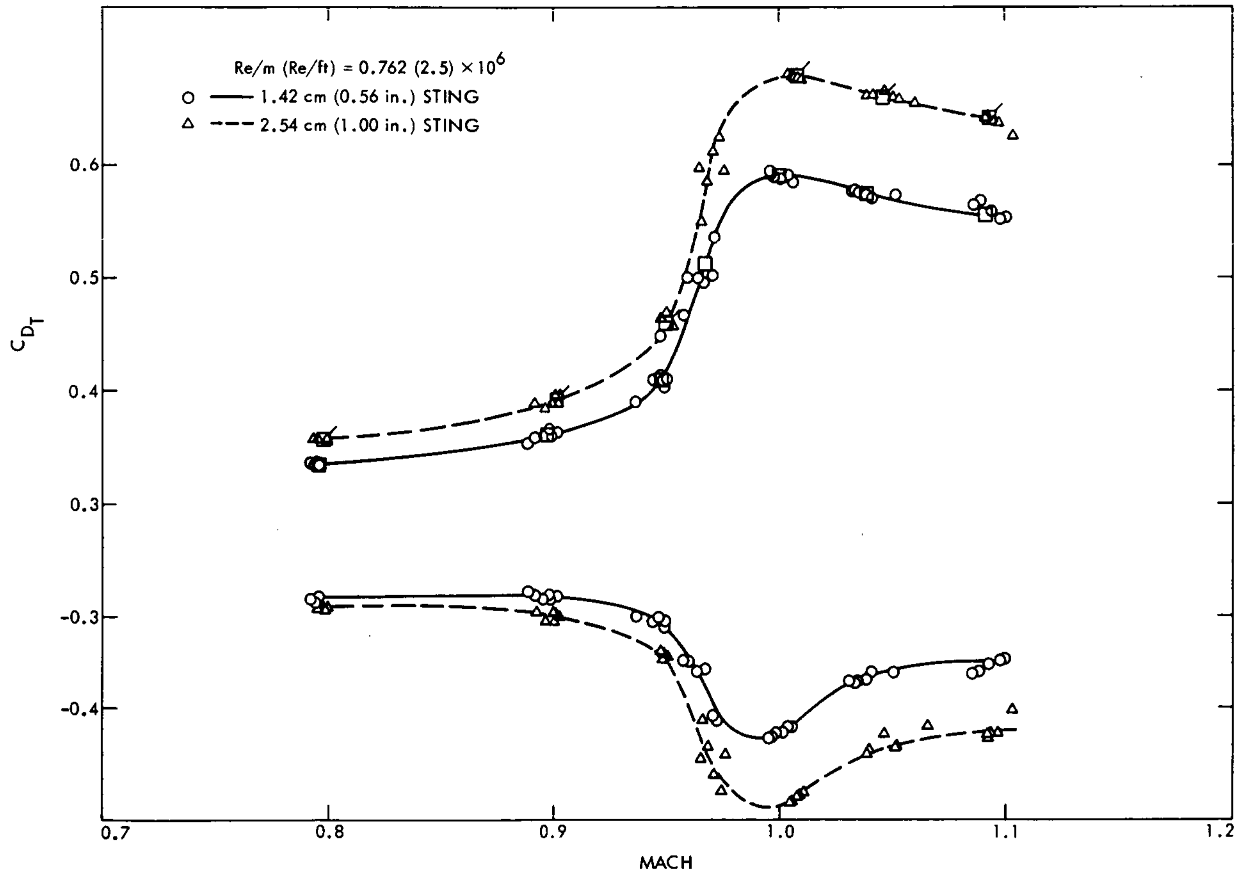

Fig. 5. 10-deg cone sting-support drag

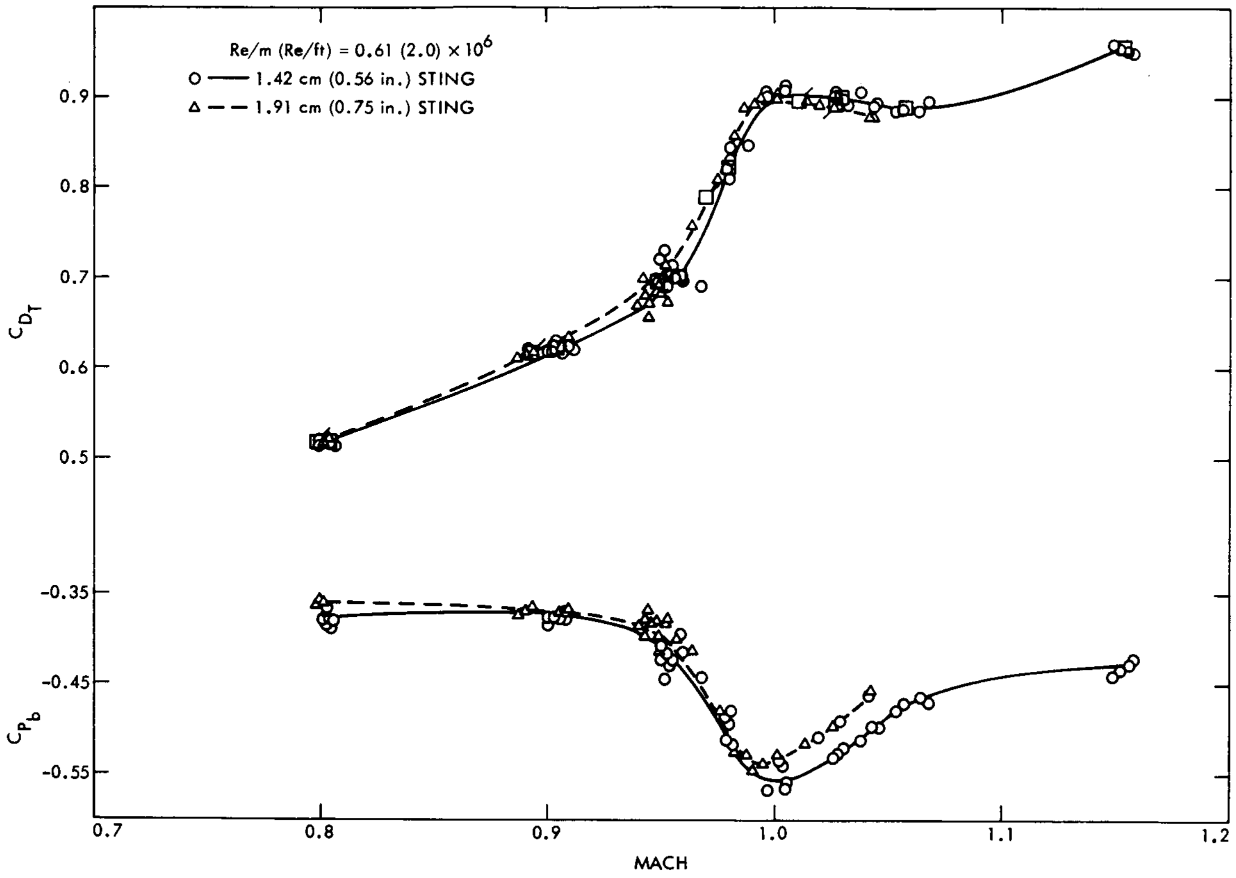

Fig. 6. Sphere sting-support drag

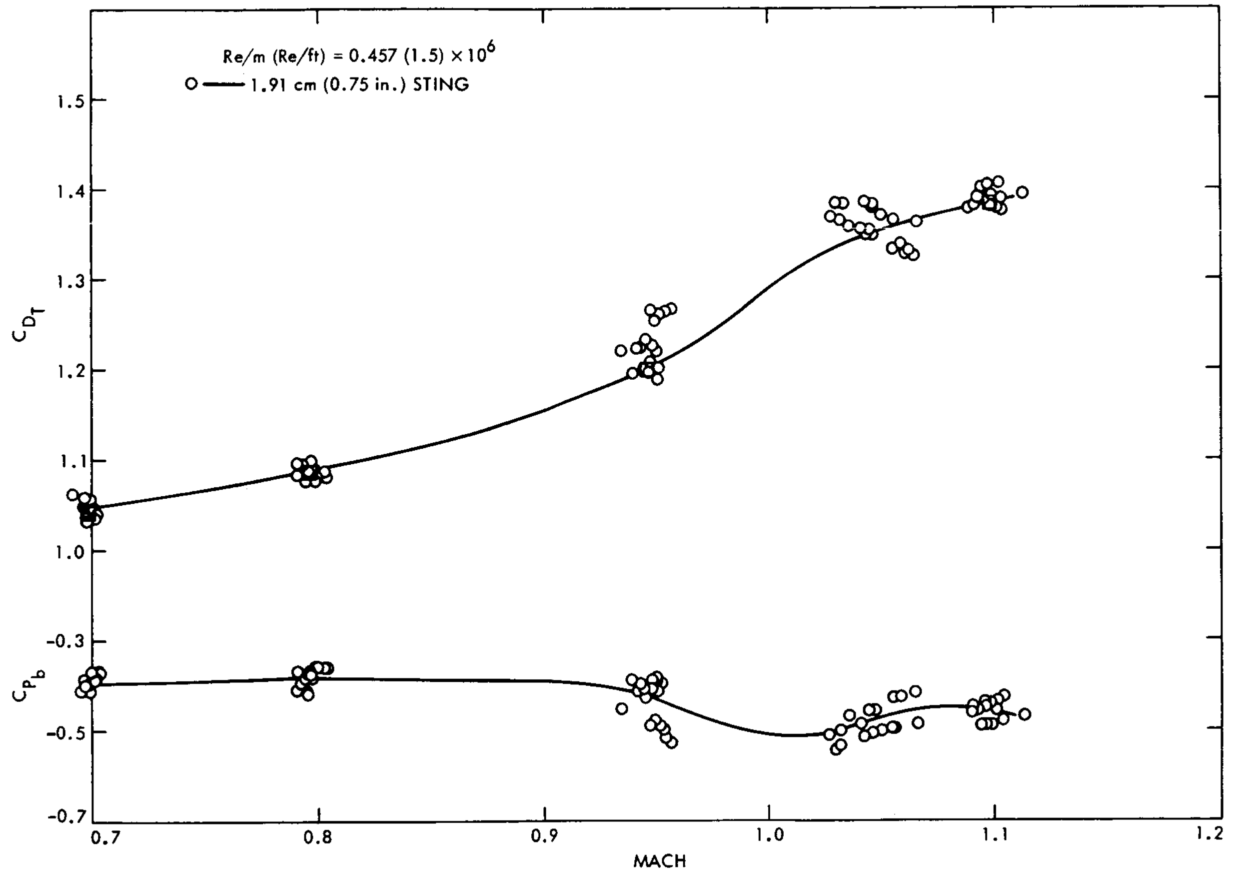

Fig. 7. 60-deg blunt cone sting-support drag

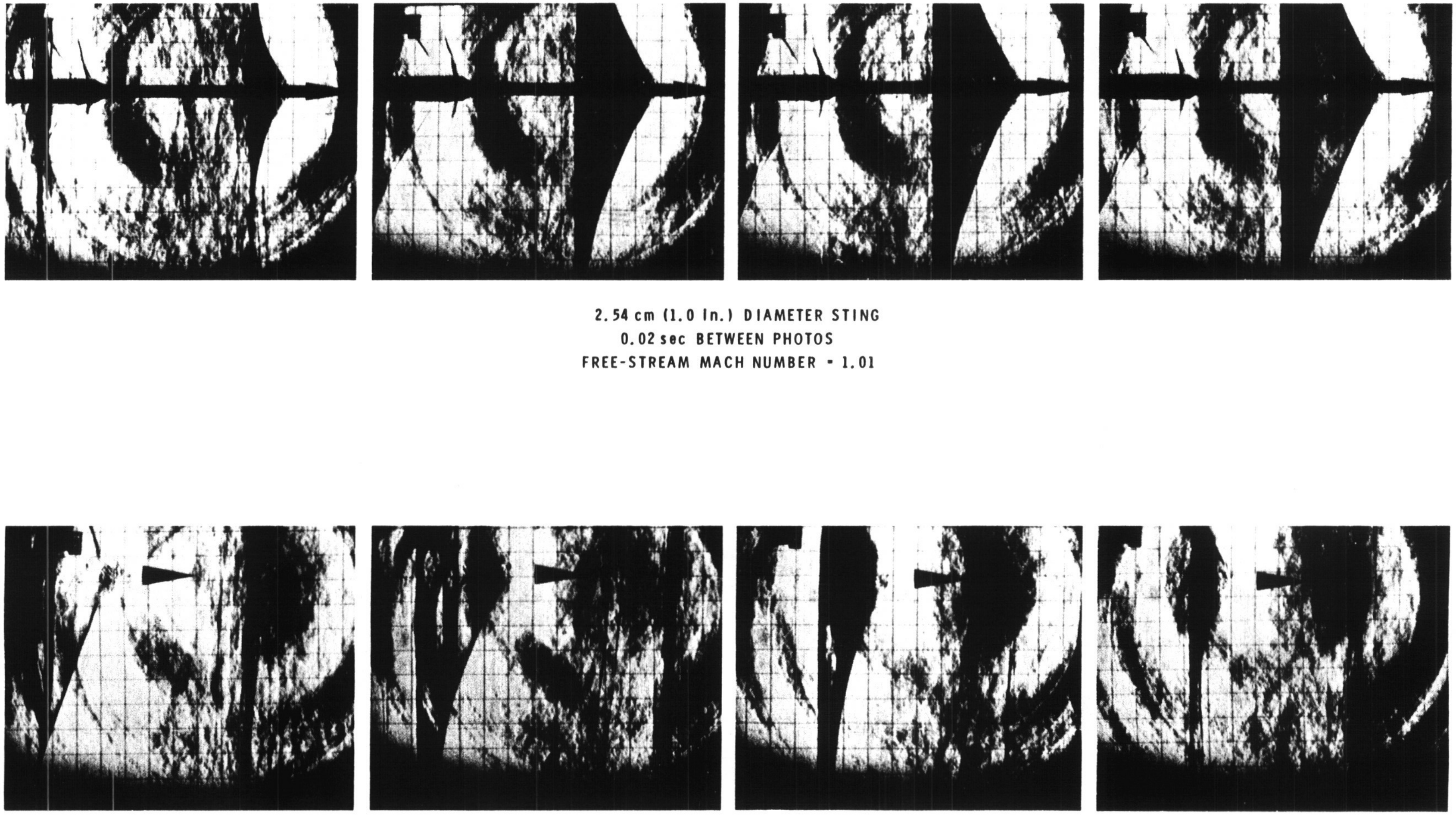

2.54 cm (1.0 in.) DIAMETER STING
0.02 sec BETWEEN PHOTOS
FREE-STREAM MACH NUMBER = 1.01

FRAME 70
MACH=1.003

FRAME 100
MACH=0.995

FRAME 130
MACH=0.987

FRAME 160
MACH=0.979

Fig. 8. Comparison of sting-support and free-flight schlieren photos with the 10-deg cone

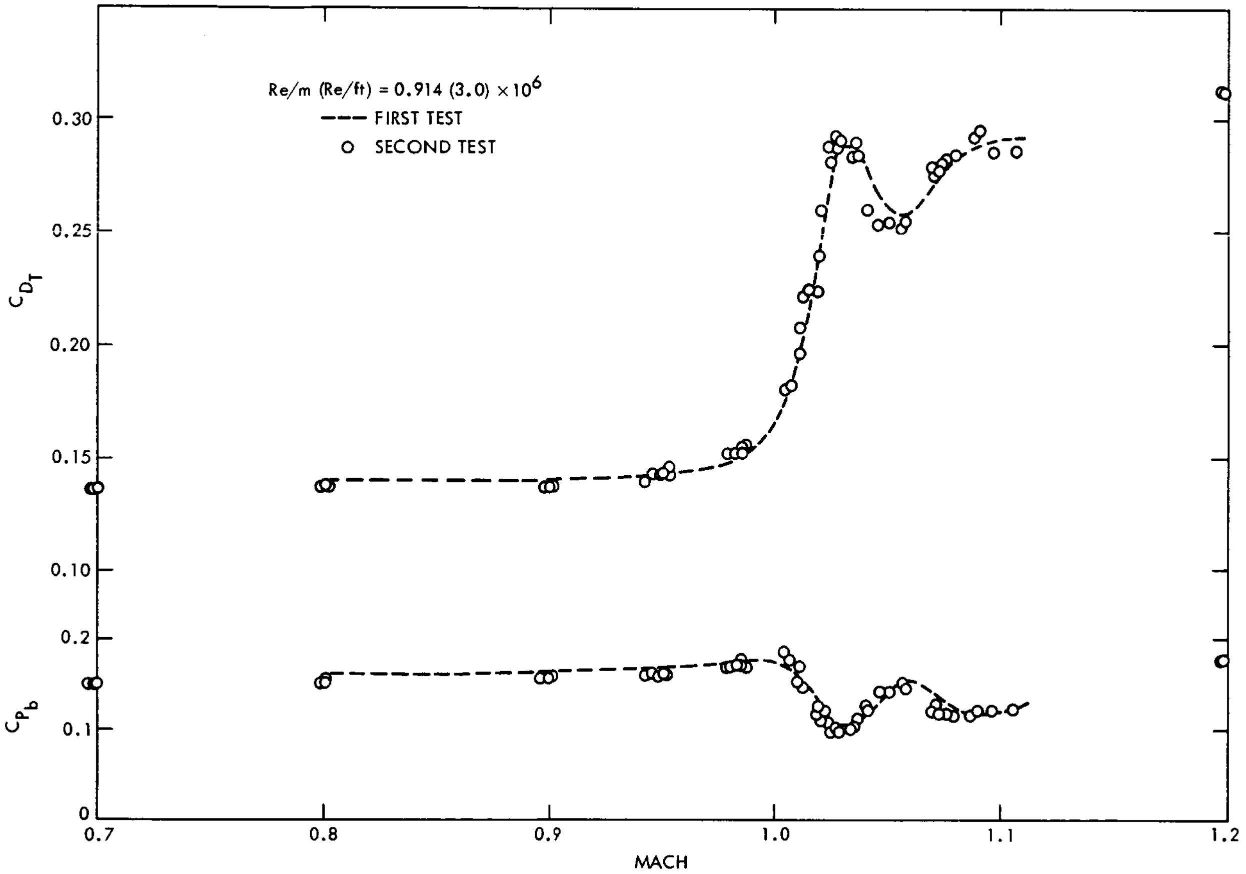

Fig. 9. Comparison of H10-F drag data from the two test periods

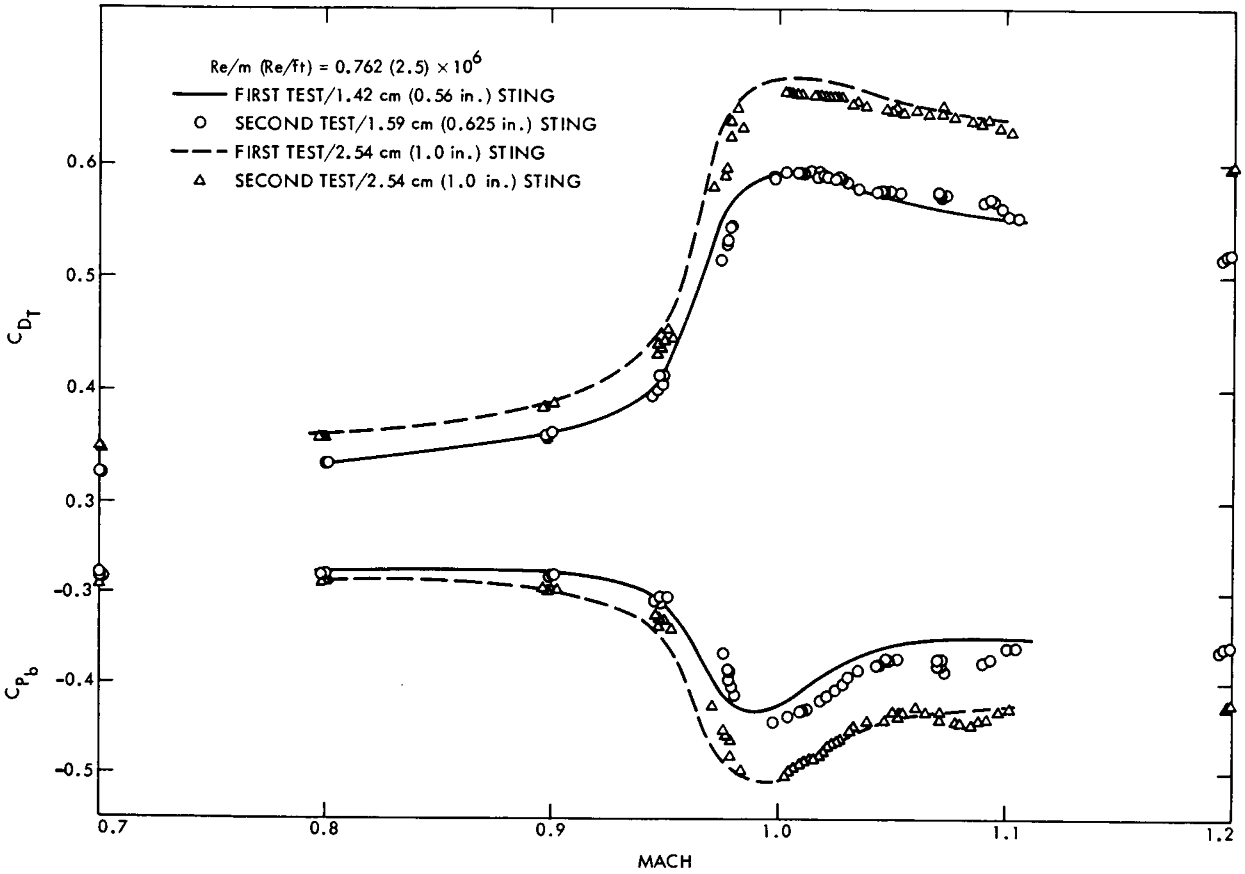

Fig. 10. Comparison of 10-deg cone drag data from the two test periods

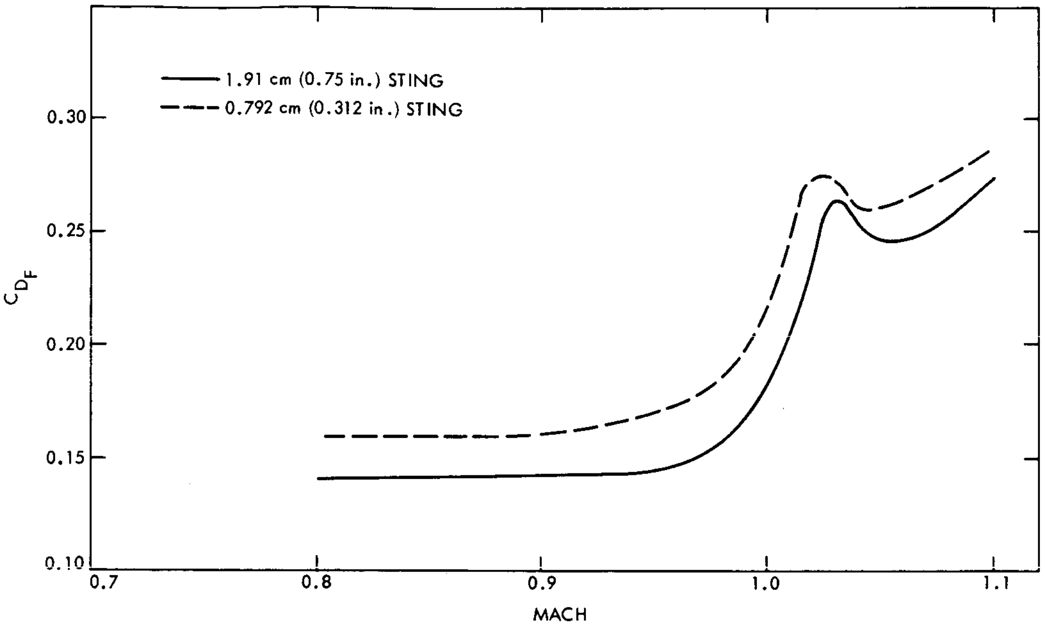

Fig. 11. Comparison of MH10-F drag data obtained with two sting diameters

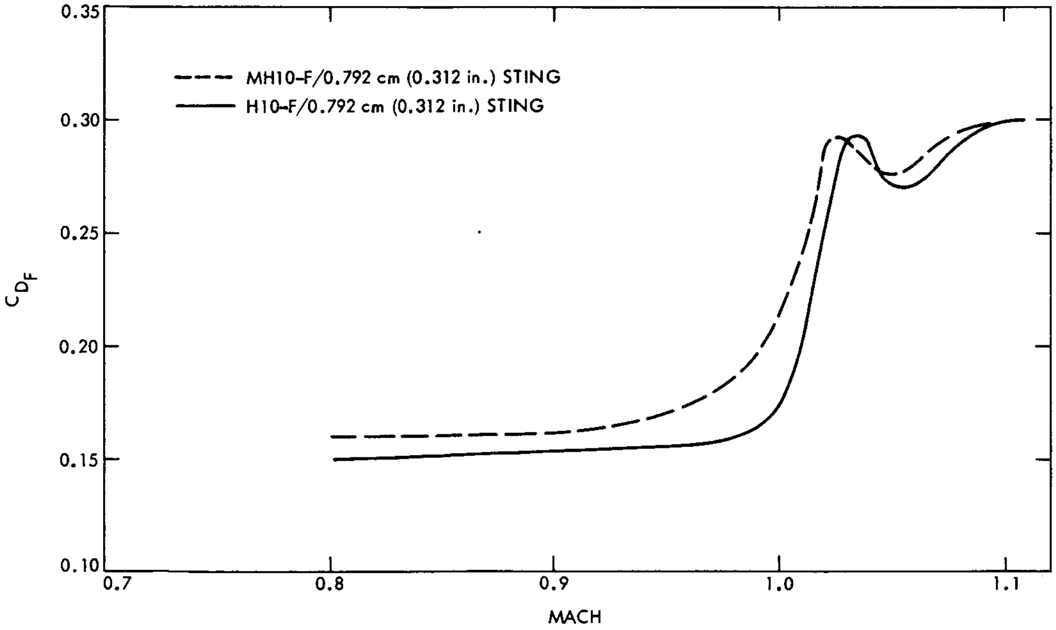

Fig. 12. Comparison of drag data from Configurations H10-F and MH10-F

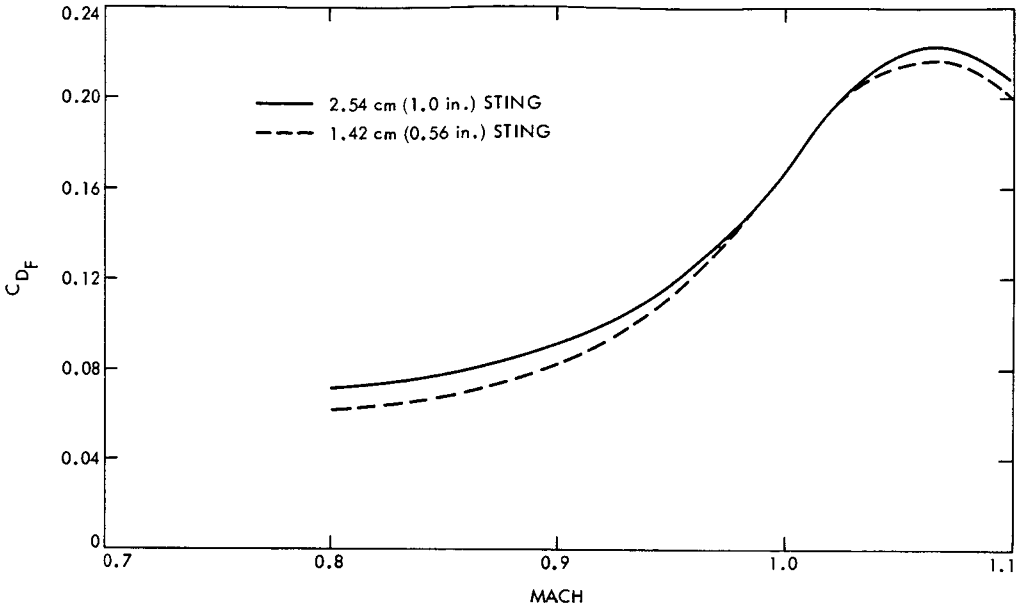

Fig. 13. Comparison of 10-deg cone drag data obtained with two sting diameters

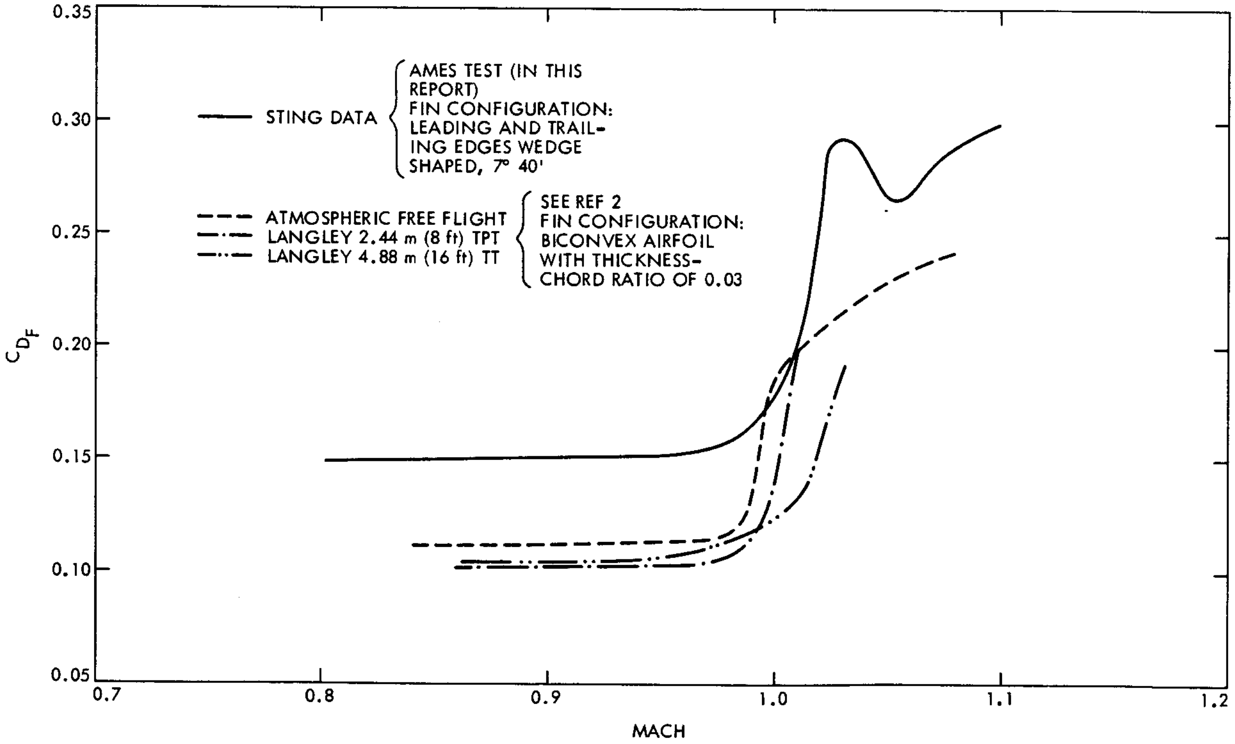

Fig. 14. Summary of H10-F drag data from different facilities

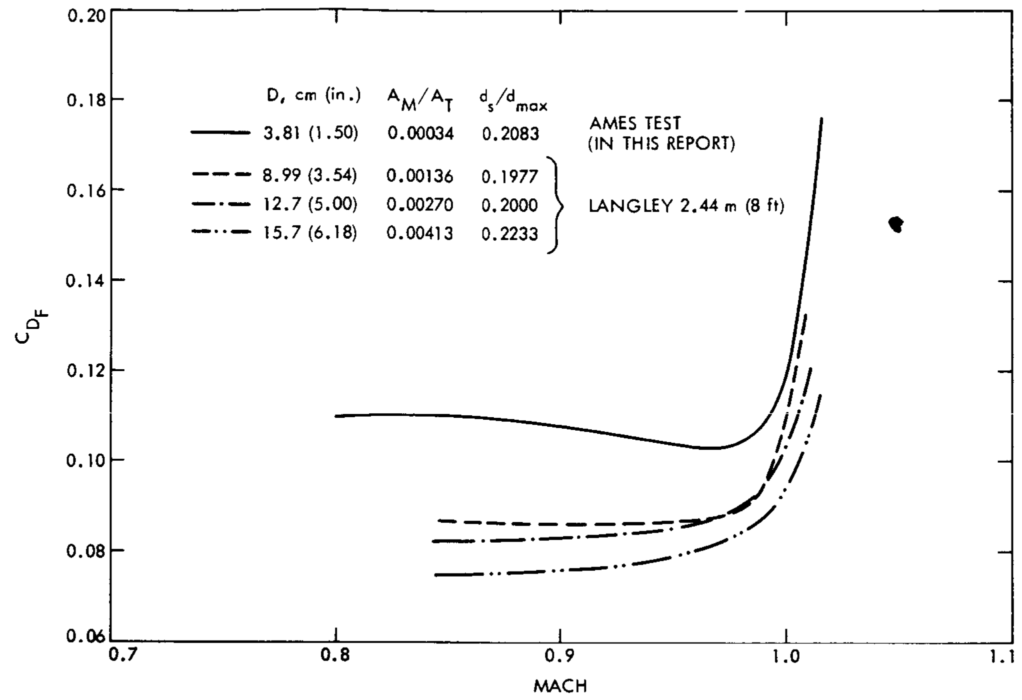

Fig. 15. Effects of blockage on Configuration H10-F

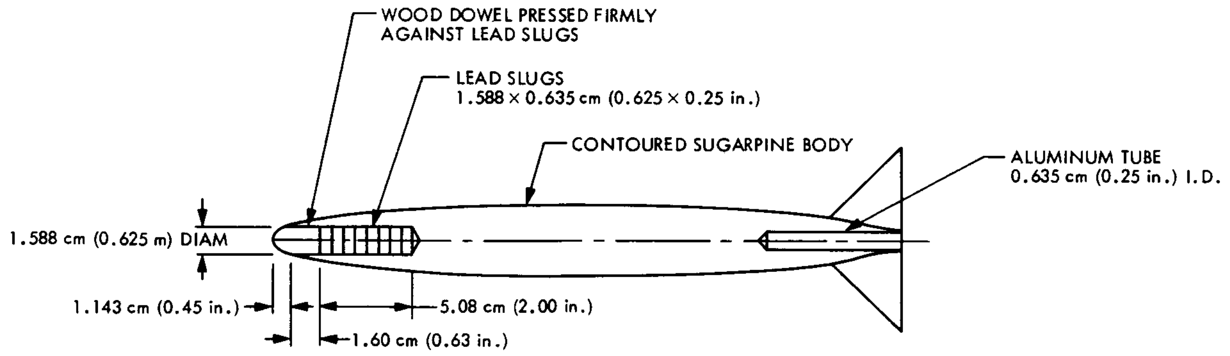

CROSS SECTION OF HIRAD MODELS

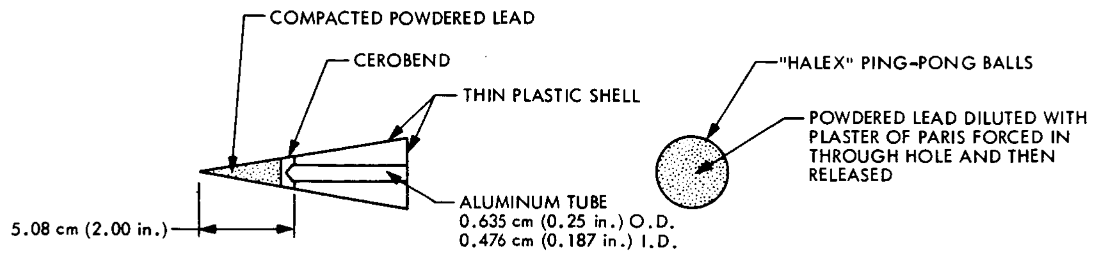

CROSS SECTION OF 10 deg CONE AND SPHERE

Fig. 16. Free-flight model construction

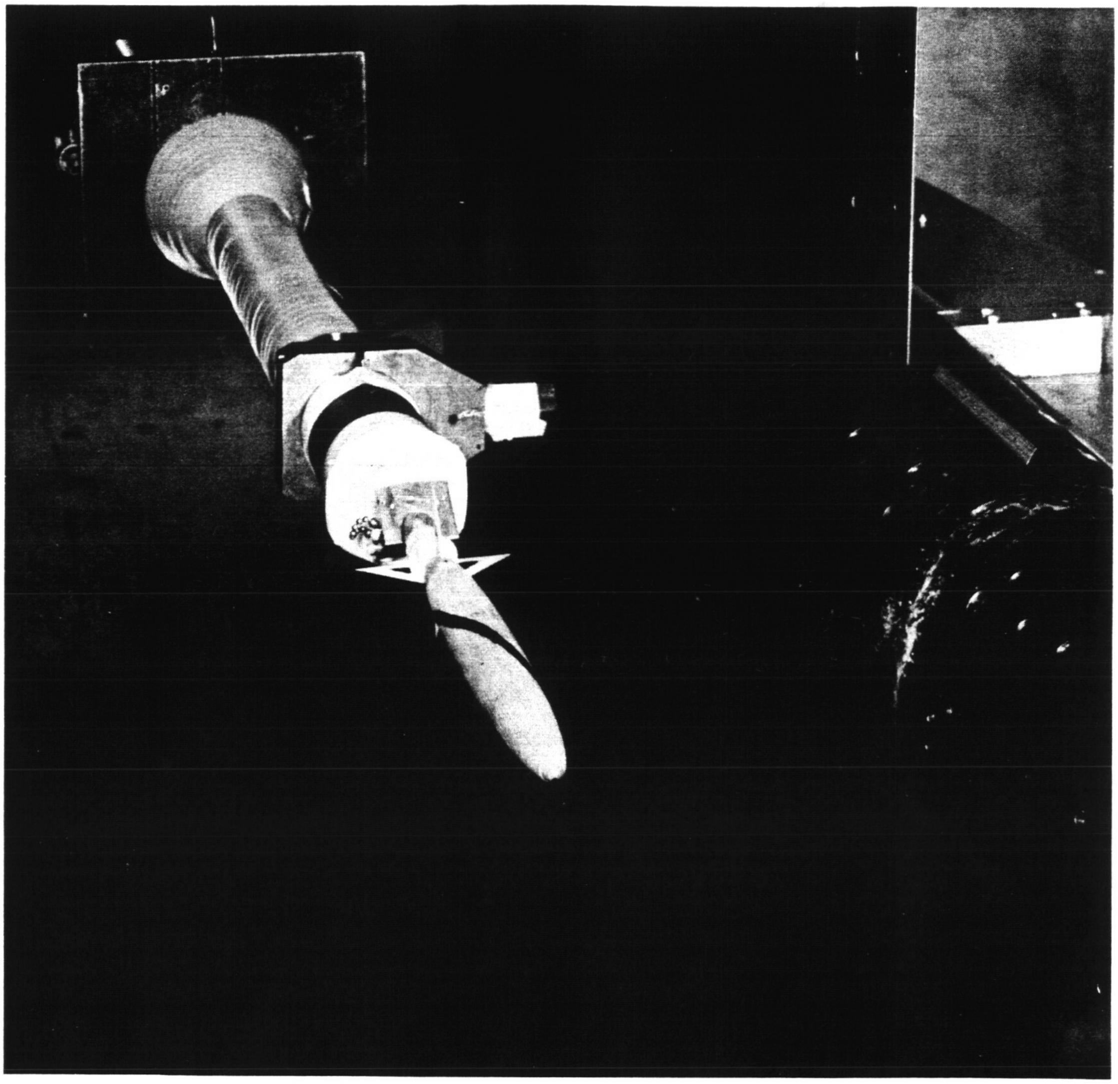

Fig. 17. Free-flight installation

(a) RUN 99, CONFIGURATION MH10-F. FREE STREAM.
MACH NUMBER 1.026. PHOTOS ARE 20 FRAMES APART.

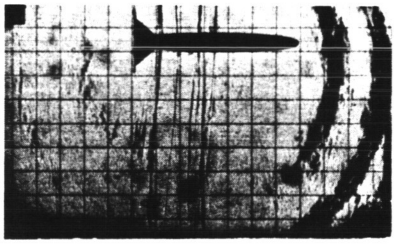

(b) RUN 86, CONFIGURATION H10-F.
NOMINAL MACH NUMBER 0.99.

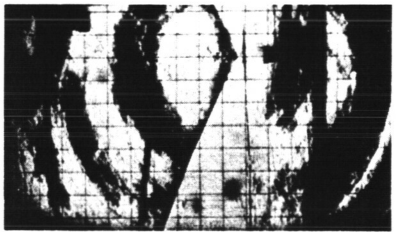

(c) RUN 119, 10-deg CONE.
NOMINAL MACH NUMBER 1.02.

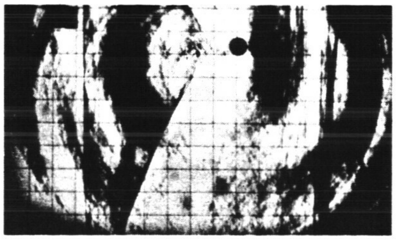

(d) RUN 90, SPHERE.
NOMINAL MACH NUMBER 0.99.

Fig. 18. Typical free-flight movie data

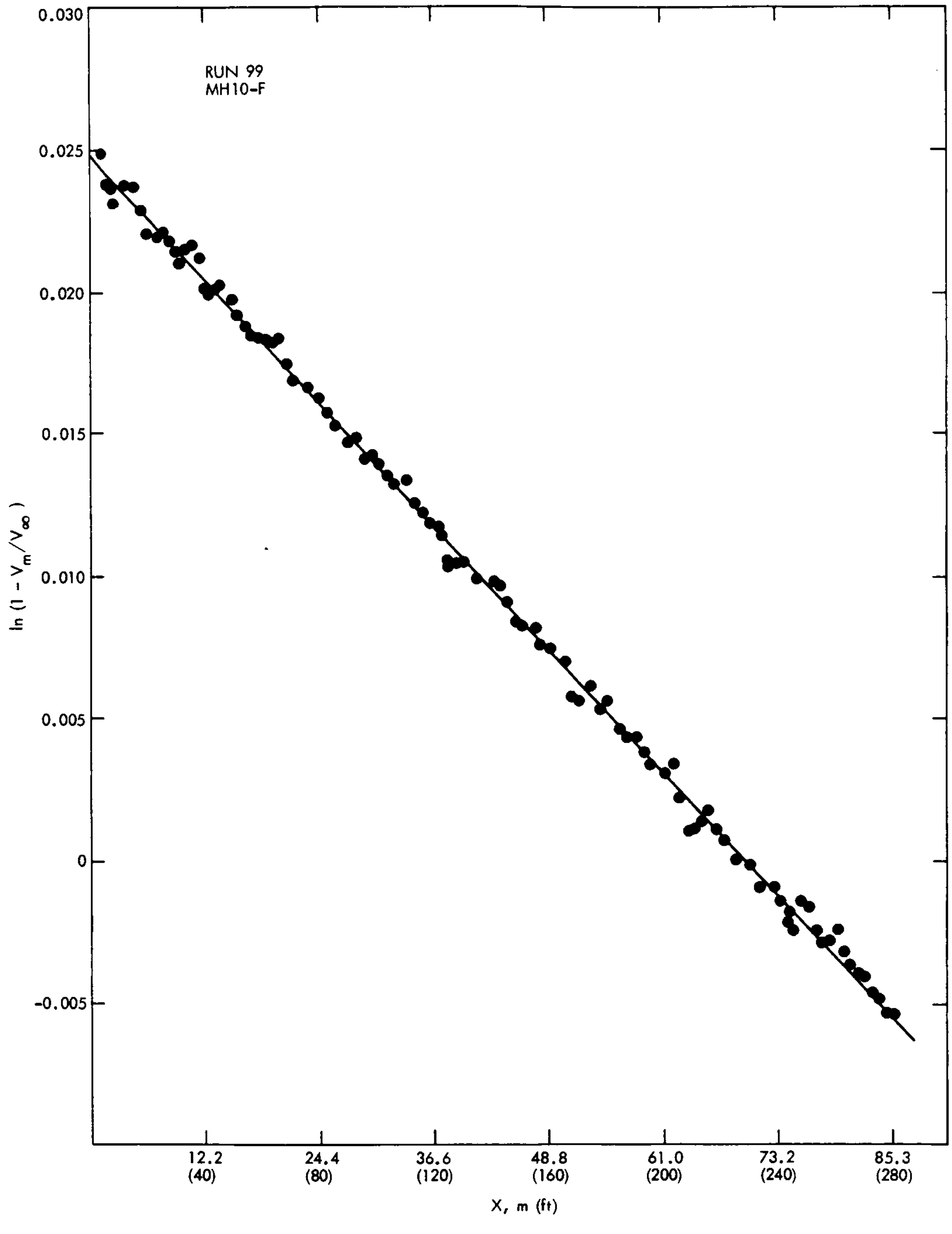

Fig. 19. Typical drag reduction ln curve

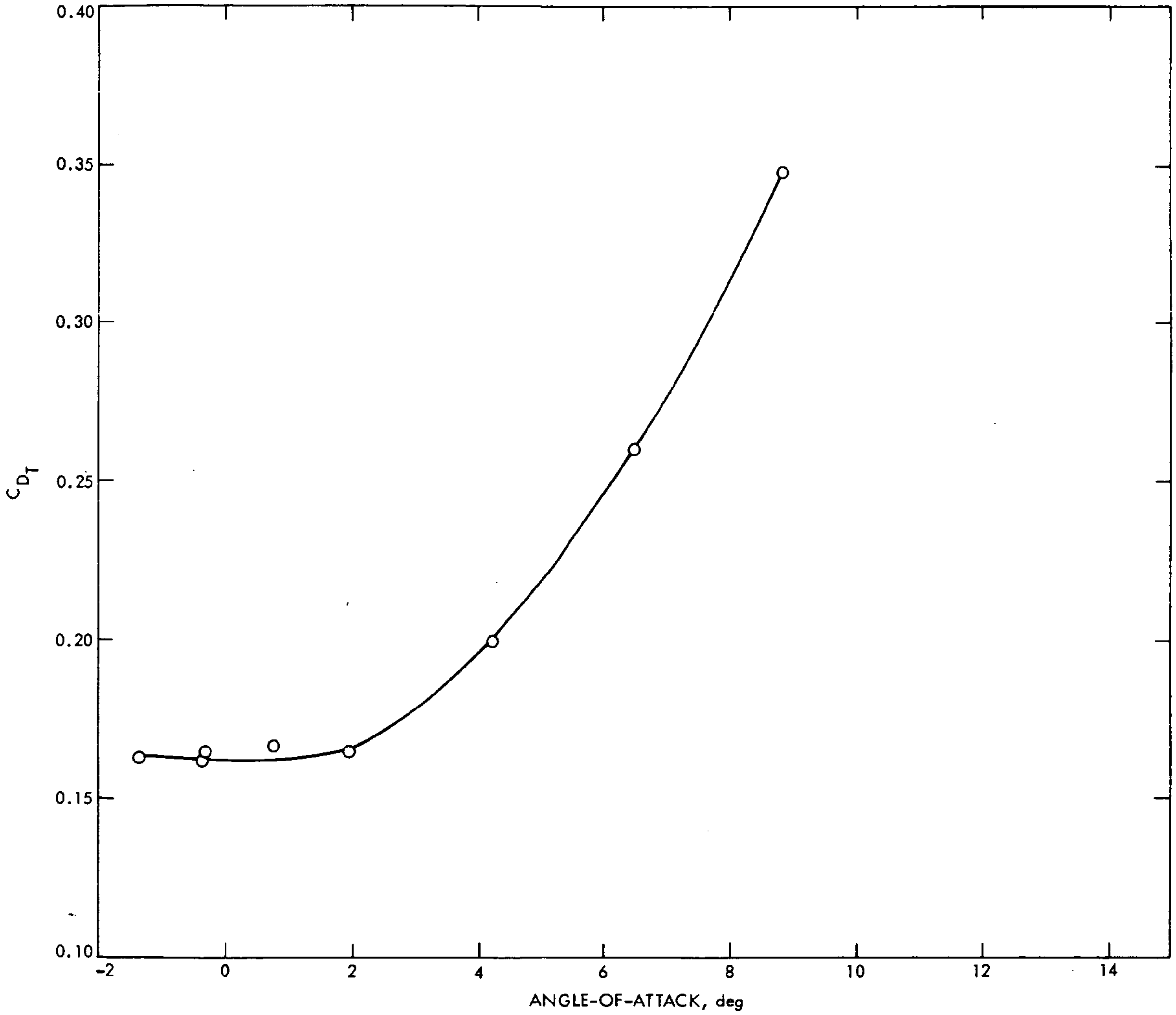

Fig. 20. Total drag versus angle-of-attack for Configuration H10-F

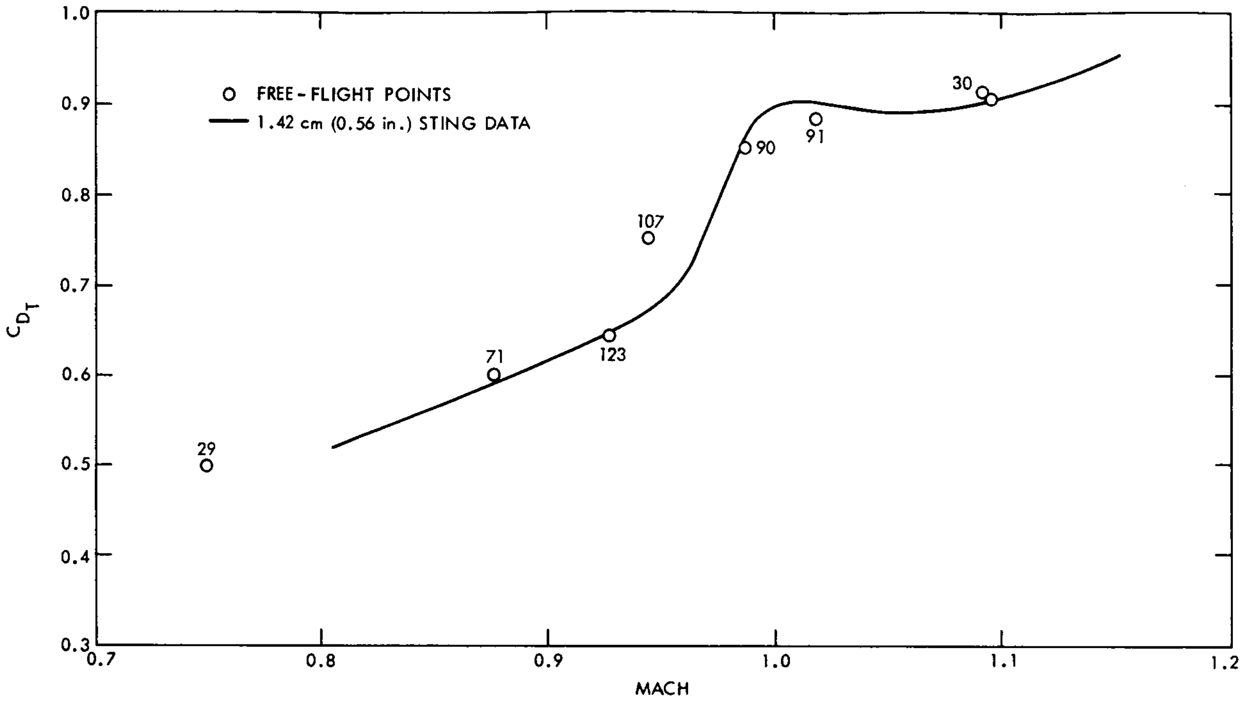

Fig. 21. Comparison of free-flight and sting-support drag for the sphere

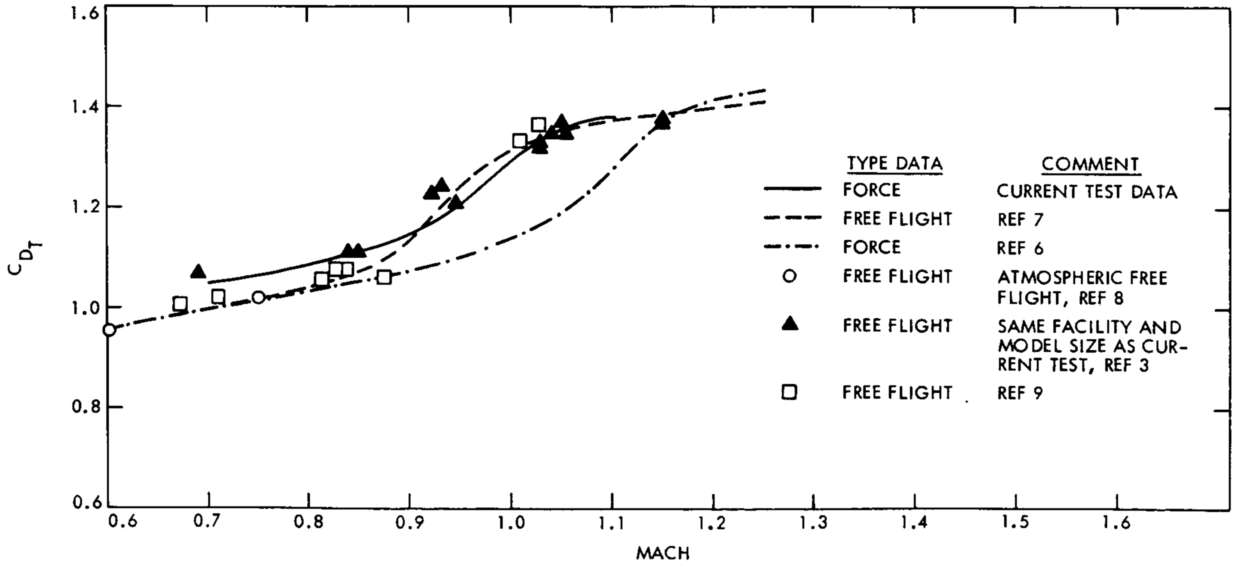

Fig. 22. Comparison of free-flight and sting-support drag for the blunt cone

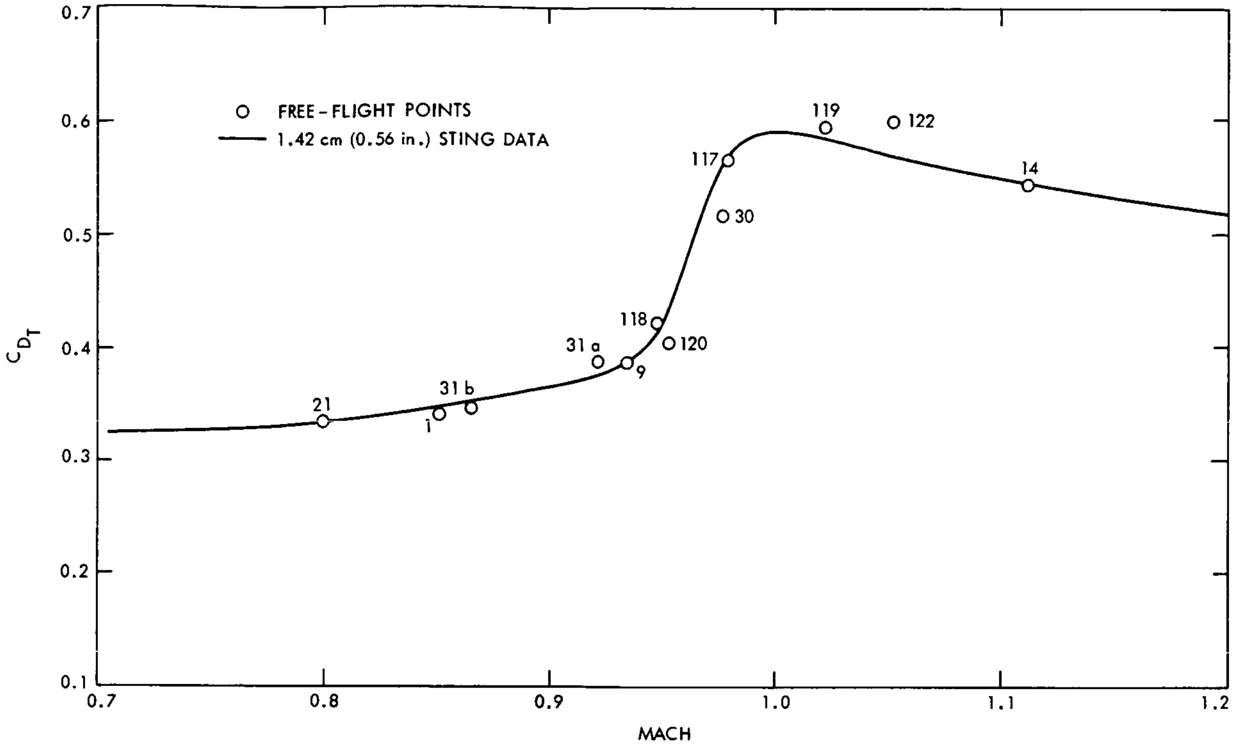

Fig. 23. Comparison of free-flight and sting-support drag for the 10-deg cone

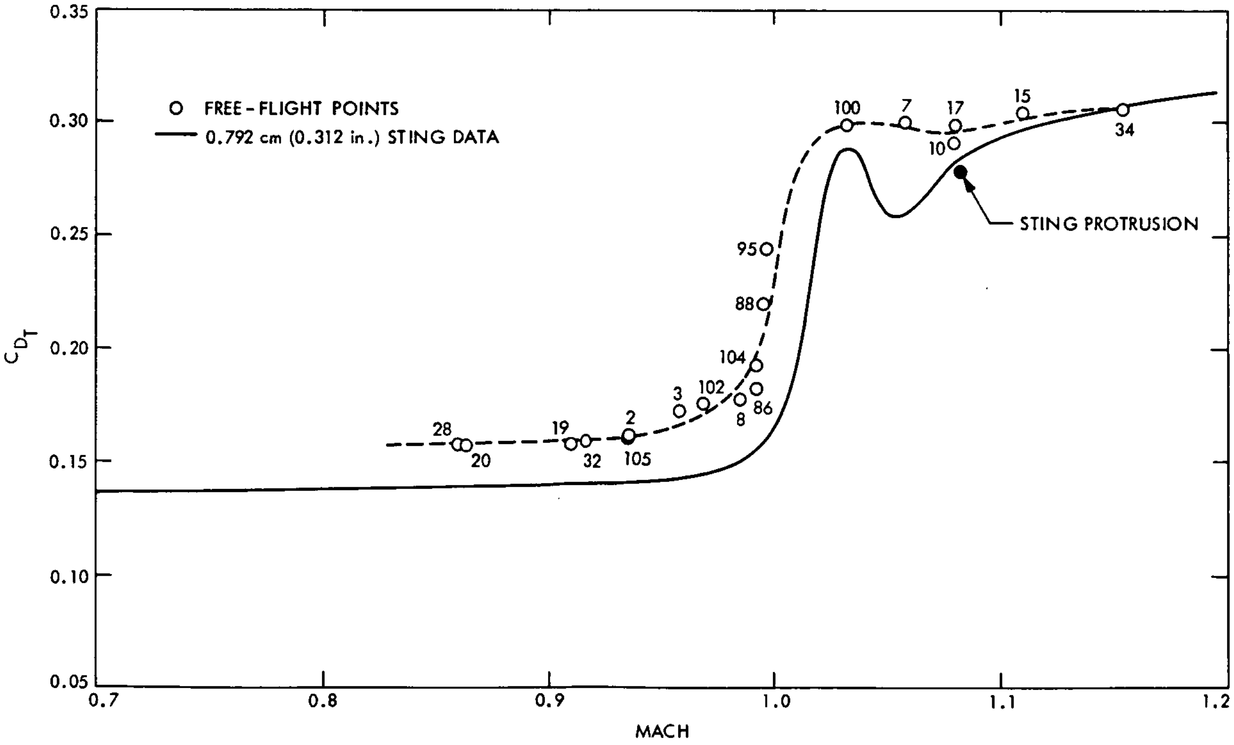

Fig. 24. Comparison of free-flight and sting-support drag for Configuration H10-F

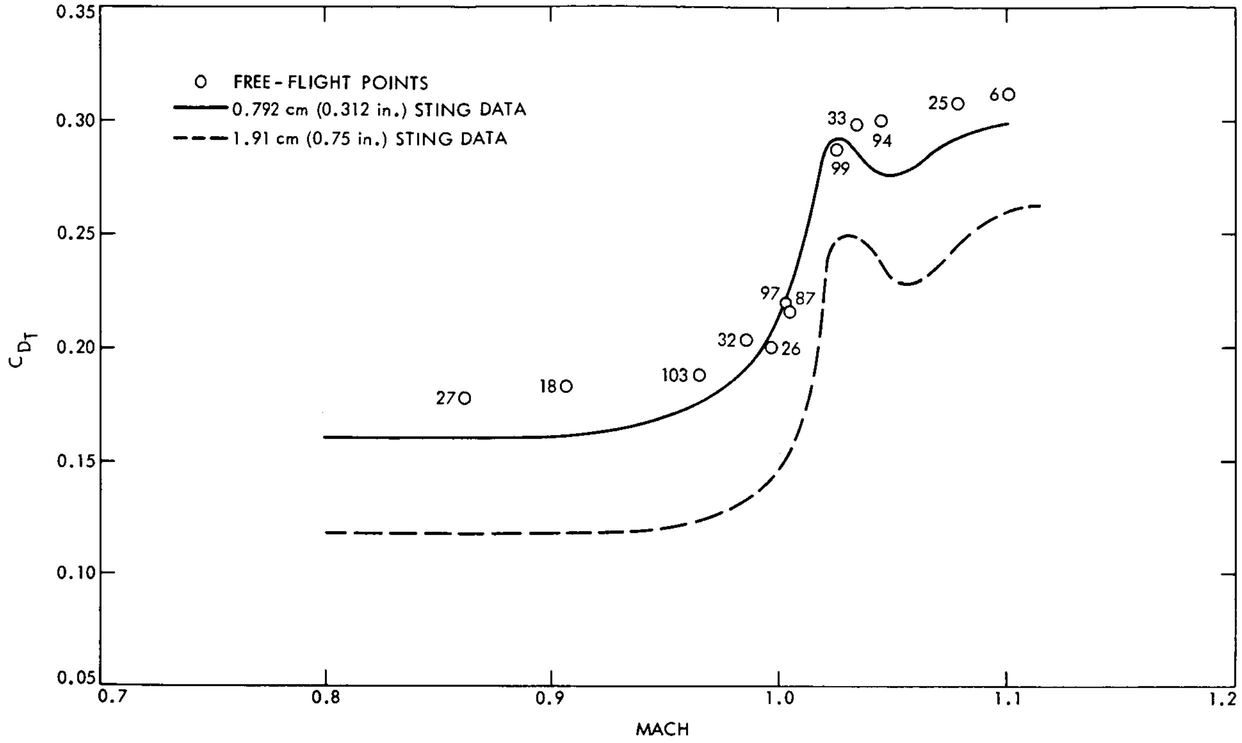

Fig. 25. Comparison of free-flight and sting-support drag for Configuration MH10-F

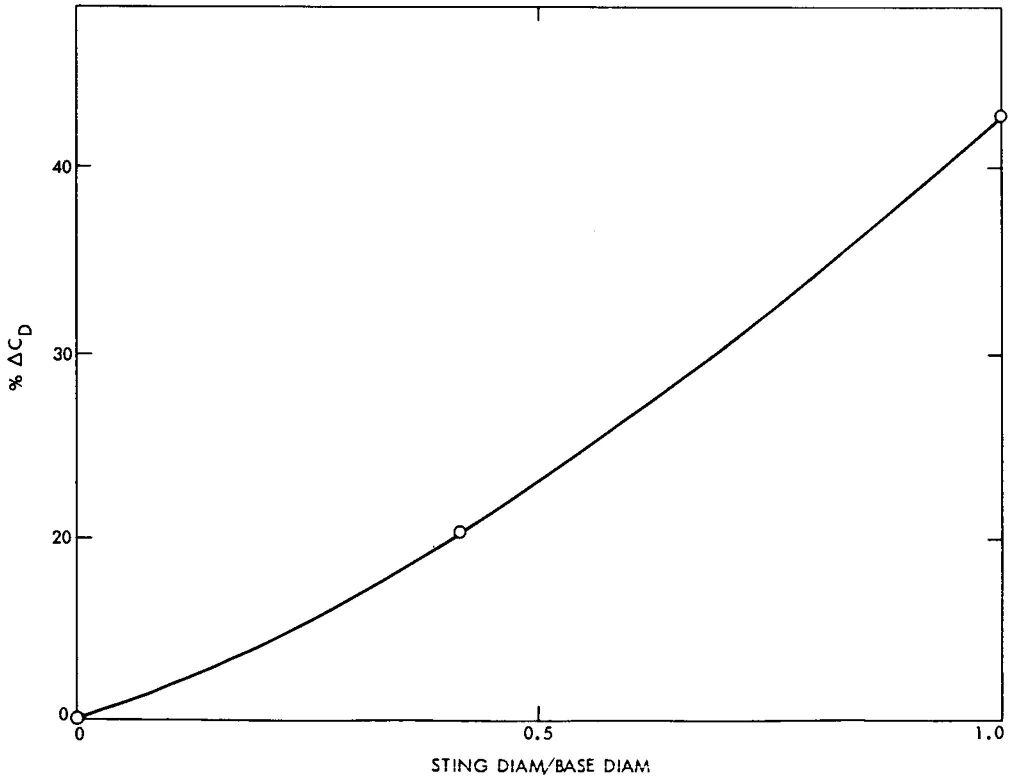

Fig. 26. Effects of sting diameter on drag for Configuration MH10-F

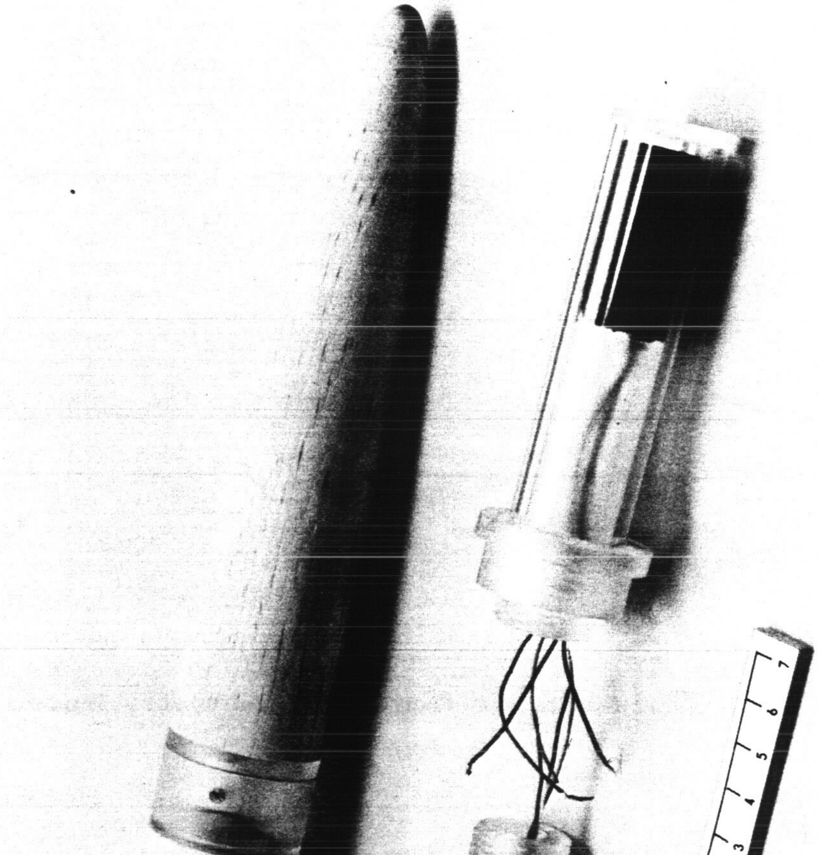

Fig. 27. H10-F telemetry model

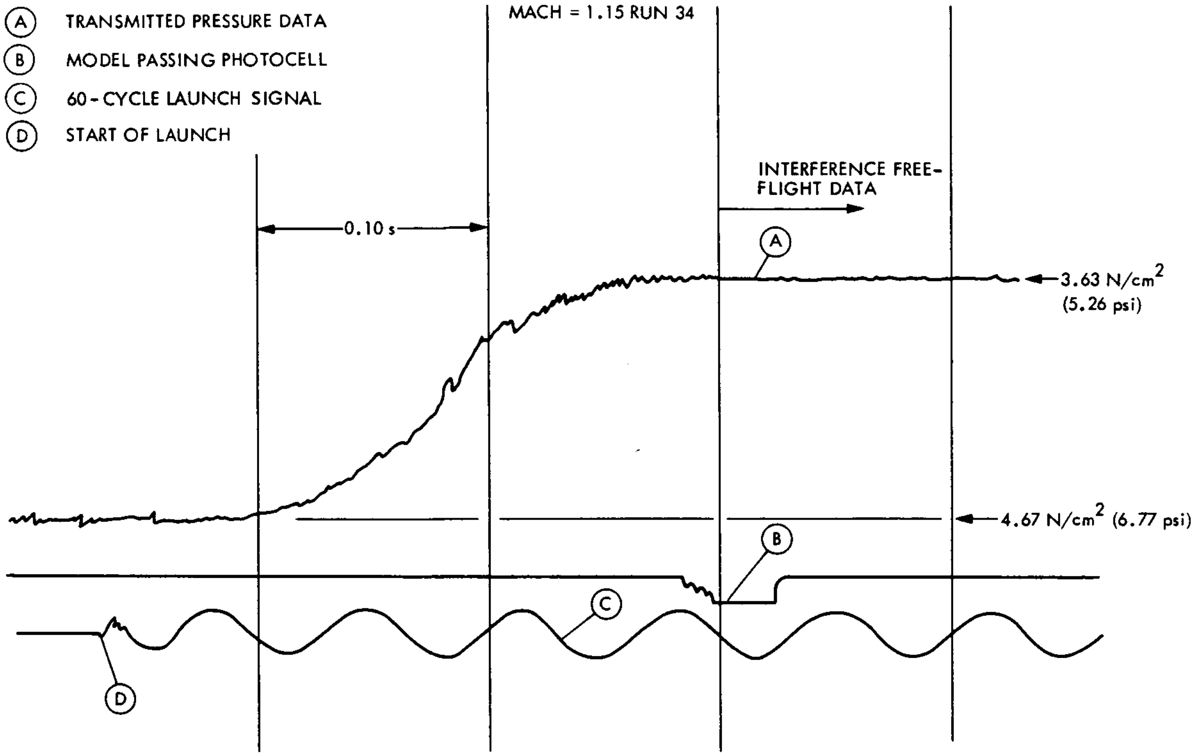

Fig. 28. Representative free-flight telemetry trace

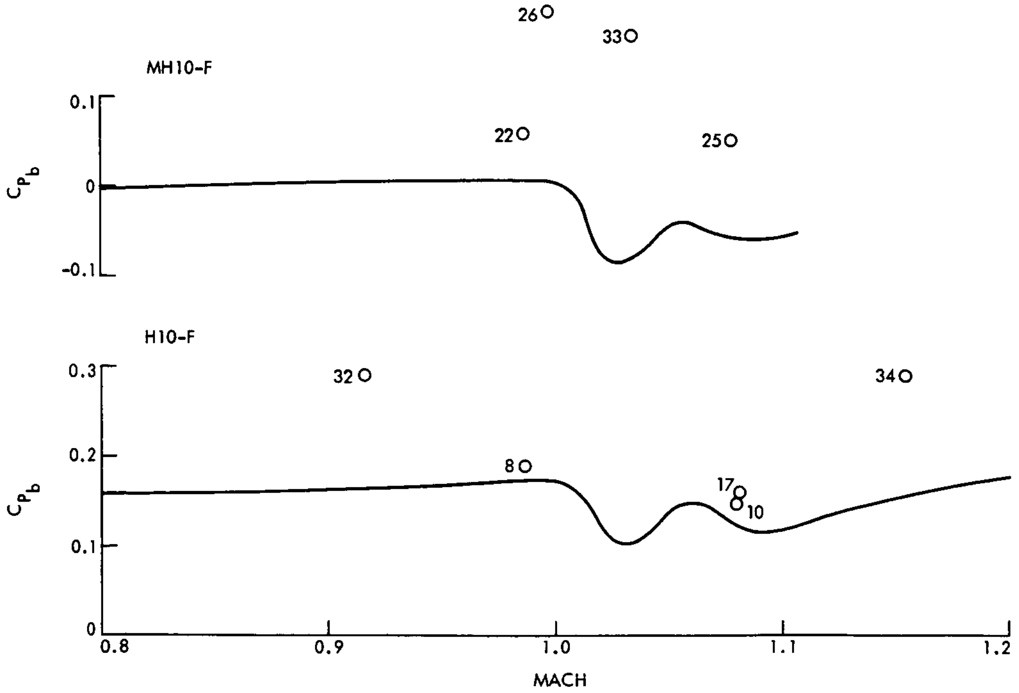

Fig. 29. Comparison of sting-support and free-flight base pressures

NASA — JPL — Coml., L.A., Calif.